


Exclusive production of quarkonia pairs in collinear factorization framework

Marat Siddikov^{*} and Iván Schmidt

*Departamento de Física, Universidad Técnica Federico Santa María,
y Centro Científico—Tecnológico de Valparaíso, Casilla 110-V, Valparaíso, Chile*

 (Received 29 December 2022; revised 31 January 2023; accepted 10 February 2023; published 28 February 2023)

In this paper, we analyze the exclusive photoproduction of heavy quarkonia pairs in the collinear factorization framework. We evaluate the amplitude of the process for the $J/\psi - \eta_c$ quarkonia pair in the leading order of the strong coupling α_s , and express it in terms of generalized parton distributions (GPDs) of gluons in the proton. We make numerical estimates in the kinematics of the Electron Ion Collider and find that, in the photoproduction regime, when the virtuality of the photon is much smaller than the quarkonia mass, the cross section of the process is sufficiently large for experimental studies. We demonstrate that the study of this channel can complement existing studies of gluon GPDs from other channels.

DOI: [10.1103/PhysRevD.107.034037](https://doi.org/10.1103/PhysRevD.107.034037)

I. INTRODUCTION

Understanding the proton structure presents one of the central problems in high-energy physics. Usually this structure is parametrized in terms of partonic and multipartonic distributions of different flavors. In view of the nonperturbative nature of strong interactions, it is not possible to evaluate these distributions theoretically from first principles, and thus we have to extract them from experimental data. For exclusive processes, the amplitudes are usually controlled by the generalized parton distributions (GPDs) of the target [1–6]. However, extraction of the GPDs from experimental data suffers from a number of technical challenges and, at present, inevitably requires the use of model assumptions, even for Compton scattering and meson production, which are considered as references in nucleon tomography [7]. Many observables might obtain simultaneous contributions of GPDs with different helicity and flavor states, albeit with different, process-dependent weights. For this reason, the extraction of partonic distributions of individual flavors inevitably requires analysis of multiple channels, and thus the extension of the number of possible channels for study of GPDs is strongly desired [8–11]. Recently a new class of $2 \rightarrow 3$ processes has been suggested in the literature [12–23], as potential new probes, which should complement existing studies, provide more

stringent constraints on existing phenomenological models, and in this way diminish theoretical uncertainty. Most of these studies focused on the production of light mesons and photons. Such processes are dominated by quark GPDs (both in chiral odd and chiral even sectors). A factorization for such processes has been proven in the kinematics when the relative transverse momenta of the produced hadrons and photon (\sim pairwise invariant masses) are large enough to avoid soft final-state interactions [24,25].

In these analyses, special attention should be paid to the extraction of gluon GPDs. Since the gluons do not couple directly to photons, they contribute to many processes only as higher-order corrections, which adversely affects the precision of the extracted gluon GPDs. However, knowledge of the gluon GPDs is important for solving many puzzles (see [1–6] for overview). The best channel for the study of gluon GPDs is the production of heavy quarkonia. Because of the expected smallness of intrinsic heavy parton densities, the process gets a dominant contribution from gluon GPDs, which might therefore be studied in detail. The heavy mass of quarkonia plays the role of a natural hard scale in the problem [26,27], relaxing the conditions on other kinematic variables and potentially opening the possibility to use perturbative methods even in the photoproduction regime. A modern nonrelativistic QCD (NRQCD) framework allows one to systematically incorporate various perturbative corrections [28–39]. The use of single quarkonia production for constraining the gluon GPDs has been discussed in detail in [40–43], and the coefficient functions have been evaluated, taking into account next-to-leading (NLO) order and some higher twist corrections. However, the amplitude of this process provides information only about GPDs convoluted with process-dependent coefficient functions, and, as mentioned

^{*}Corresponding author.
marat.siddikov@usm.cl

Published by the American Physical Society under the terms of the Creative Commons Attribution 4.0 International license. Further distribution of this work must maintain attribution to the author(s) and the published article's title, journal citation, and DOI. Funded by SCOAP³.

earlier, an inversion of the procedure might be impossible, especially when the complicated structure of higher-order corrections is taken into account. For this reason, it is important to complement the analysis with data from other channels. A natural and straightforward extension of these studies is the production of multiple quarkonia (e.g., heavy quarkonia pairs). Such processes have been the subject of theoretical studies since the early days of QCD [44–47] and recently got renewed interest due to the forthcoming launch of high-luminosity accelerator facilities, as well as being a potential gateway for the study of all-heavy tetraquarks, which might be molecular states of quarkonia pairs [48–58].

Previously, the exclusive production of quarkonia pairs has been studied for $J/\psi J/\psi$ production, which might proceed only via a two-photon mechanism $\gamma\gamma \rightarrow M_1 M_2$ [59–64] due to C -parity constraints and thus cannot be used for studies of gluon GPDs. Recently, we analyzed the production of quarkonia pairs with opposite C -parities, which proceeds via photon-pomeron fusion and thus have larger cross sections [65]. However, our study was realized in the framework of the color glass condensate approach and relied on an underlying eikonal picture, which is valid in the small- x domain. At smaller energies, as well as in the kinematics of large photon virtuality Q^2 , the assumptions of this picture are not well justified, and it makes sense to analyze this process in the complementary collinear factorization approach, which is expected to give reasonable predictions in this kinematics and give access to the aforementioned gluon GPDs of the target. This kinematic regime might be studied in low-energy electron-proton collisions at the forthcoming Electron Ion Collider (EIC) [66–69].

The paper is structured as follows. Below, in Sec. II, we discuss in detail the kinematics of the process and the framework for the evaluation of the amplitude of the process. In Sec. III, we present our numerical estimates for the cross sections, in EIC kinematics. Finally, in Sec. IV, we draw conclusions.

II. EXCLUSIVE PHOTOPRODUCTION OF MESON PAIRS

Previously, the exclusive production of *light* meson pairs was analyzed in Bjorken kinematics in [70–74], with the additional constraint that the invariant mass of the meson pair should be large. There it was demonstrated that the amplitude of that process might be represented as a convolution of the quark and gluon GPDs of the target, with novel two-meson distribution amplitudes. However, the extension of those results to quarkonia pairs is not straightforward, since quarkonia masses and the invariant mass \mathcal{M}_{12} are very large, so the Bjorken regime ($Q \gg \mathcal{M}_{12}$) is achieved in the kinematics where the cross section is negligibly small. For this reason, it makes sense to analyze the quarkonia pair production by treating the

heavy mass of the quark and the photon virtuality Q as two independent hard scales, with the photoproduction ($Q \ll \mathcal{M}_{12}$) and Bjorken ($Q \gg \mathcal{M}_{12}$) regimes as limiting cases. In the following Sec. II A we discuss in detail the kinematics of the process, and in Sec. II B we discuss the evaluation of the amplitudes in the collinear factorization approach and their relation to the target gluon GPDs.

A. Kinematics of the process

In order to facilitate the comparison with experimental data, in what follows we will present our results in the frame whose axis z coincides with the photon-proton collision axis, so the light-cone decomposition of the momenta is given by

$$q = \left(-\frac{Q^2}{2q^-}, q^-, \mathbf{0}_\perp \right), \quad q^- = E_\gamma + \sqrt{E_\gamma^2 + Q^2}, \quad (1)$$

$$P = \left(P^+, \frac{m_N^2}{2P^+}, \mathbf{0}_\perp \right), \quad P^+ = E_p + \sqrt{E_p^2 - m_N^2}, \quad (2)$$

$$p_a = \left(\frac{M_a^\perp}{2} e^{-y_a}, M_a^\perp e^{y_a}, \mathbf{p}_a^\perp \right), \quad a = 1, 2, \quad (3)$$

$$M_a^\perp \equiv \sqrt{M_a^2 + (\mathbf{p}_a^\perp)^2}, \quad (4)$$

where q is the (virtual) photon momentum, P and P' are the momenta of the proton before and after the collision, and p_1, p_2 are the 4-momenta of the produced heavy quarkonia; the latter are expressed in terms of the rapidities and transverse momenta (y_a, \mathbf{p}_a^\perp) of these heavy mesons. This frame allows for straightforward analysis down to the photoproduction limit ($Q \rightarrow 0$). The relation of this frame to the so-called symmetric frame [2,3,73,75–79], which is used for the analysis in Bjorken kinematics ($Q \rightarrow \infty$), is discussed in detail in Appendix A. In the limit $Q \rightarrow 0$, this frame, up to a trivial longitudinal boost, coincides with the frame used in earlier studies of exclusive photoproduction $\gamma p \rightarrow \gamma M p$ [12–21]. In this frame, the polarization vectors of the longitudinally and transversely polarized photons are chosen respectively as¹

$$\varepsilon_L = \left(\frac{Q}{q}, 0, \mathbf{0}_\perp \right), \quad \varepsilon_T^{(\pm)} = \left(0, 0, \frac{1}{\sqrt{2}}, \pm \frac{i}{\sqrt{2}} \right). \quad (5)$$

We also will use the notations

¹We have chosen the longitudinal vector in the light-cone gauge, so the contribution of the longitudinal photons in the ep amplitude might be reinterpreted as an instantaneous part of the photon propagator. The results will not change under any redefinition of polarization vectors $\varepsilon_\mu(q) \rightarrow \varepsilon_\mu(q) + \text{const } q_\mu$ in view of the Ward identity (in this problem, it remains valid even for off-shell photons, since all amplitudes with an omitted photon vertex vanish due to C parity).

$$\Delta = P' - P = q - p_1 - p_2 = (\Delta^+, \Delta^-, \Delta^\perp), \quad (6)$$

$$\Delta^+ = -\frac{Q^2}{2q^-} - \frac{M_1^\perp e^{-y_1}}{2} - \frac{M_2^\perp e^{-y_2}}{2},$$

$$\Delta^- = q^- - M_1^\perp e^{y_1} - M_2^\perp e^{y_2}, \quad \Delta_\perp = -\mathbf{p}_1^\perp - \mathbf{p}_2^\perp \quad (7)$$

for the four-vector of momentum transfer to the proton and its components, and the notation t for its square,

$$t = \Delta^2 = -(q^- - M_1^\perp e^{y_1} - M_2^\perp e^{y_2})$$

$$\times \left(\frac{Q^2}{q^-} + M_1^\perp e^{-y_1} + M_2^\perp e^{-y_2} \right) - (\mathbf{p}_1^\perp + \mathbf{p}_2^\perp)^2$$

$$= -Q^2 + M_1^2 + M_2^2 - q^- (M_1^\perp e^{-y_1} + M_2^\perp e^{-y_2})$$

$$+ \frac{Q^2}{q^-} (M_1^\perp e^{y_1} + M_2^\perp e^{y_2})$$

$$+ 2(M_1^\perp M_2^\perp \cosh \Delta y - \mathbf{p}_1^\perp \cdot \mathbf{p}_2^\perp). \quad (8)$$

After the interaction, the 4-momentum of the proton is given by

$$P' = P + \Delta = \left(q^- + \frac{m_N^2}{2P^+} - M_1^\perp e^{y_1} - M_2^\perp e^{y_2}, P^+ - \frac{Q^2}{2q^-} \right. \\ \left. - \frac{M_1^\perp e^{-y_1} + M_2^\perp e^{-y_2}}{2}, -\mathbf{p}_1^\perp - \mathbf{p}_2^\perp \right), \quad (9)$$

and the on-shellness condition $(P + \Delta)^2 = m_N^2$ allows one to get an additional constraint

$$q^- P^+ = P^+ (M_1^\perp e^{y_1} + M_2^\perp e^{y_2}) - \frac{m_N^2 + t}{2} + \frac{m_N^2}{4P^+}$$

$$\times \left(M_1^\perp e^{-y_1} + M_2^\perp e^{-y_2} + \frac{Q^2}{q^-} \right). \quad (10)$$

Solving Eq. (10) with respect to q^- , we get

$$q^- = \frac{M_1^\perp e^{y_1} + M_2^\perp e^{y_2} - \frac{m_N^2 + t}{2P^+} + \frac{m_N^2}{4(P^+)^2} (M_1^\perp e^{-y_1} + M_2^\perp e^{-y_2})}{2}$$

$$+ \frac{1}{2} \sqrt{\left(M_1^\perp e^{y_1} + M_2^\perp e^{y_2} - \frac{m_N^2 + t}{2P^+} + \frac{m_N^2}{4(P^+)^2} (M_1^\perp e^{-y_1} + M_2^\perp e^{-y_2}) \right)^2 + \frac{Q^2 m_N^2}{(P^+)^2}}, \quad (11)$$

which allows us to express the energy of the photon $E_\gamma \approx q^-/2$ in terms of the kinematic variables $(y_a, \mathbf{p}_a^\perp)$ of the produced quarkonia. For asymptotically large energies $q^-, P^+ \gg \{Q, M_a, m_N, \sqrt{|t|}\}$, the result (11) reduces to

$$q^- \approx M_1^\perp e^{y_1} + M_2^\perp e^{y_2}, \quad (12)$$

and in this limit the variable t merely reduces to

$$t \approx -(\mathbf{p}_1^\perp + \mathbf{p}_2^\perp)^2. \quad (13)$$

In the photoproduction regime, the expression for q^- simplifies to

$$q^- = M_1^\perp e^{y_1} + M_2^\perp e^{y_2} - \frac{m_N^2 + t}{2P^+} + \frac{m_N^2}{4(P^+)^2}$$

$$\times (M_1^\perp e^{-y_1} + M_2^\perp e^{-y_2}). \quad (14)$$

The invariant energy W of the γp collision and the invariant mass \mathcal{M}_{12} of the produced heavy quarkonia pair in terms of these variables might be rewritten as

$$W^2 \equiv s_{\gamma p} = (q + P)^2 = -Q^2 + m_N^2 + 2q \cdot P, \quad (15)$$

and

$$\mathcal{M}_{12}^2 = (p_1 + p_2)^2 = M_1^2 + M_2^2$$

$$+ 2(M_1^\perp M_2^\perp \cosh \Delta y - \mathbf{p}_1^\perp \cdot \mathbf{p}_2^\perp)$$

$$= t - Q^2 + 2M_1^\perp Q \cosh(y_1 + \delta y_q)$$

$$+ 2M_2^\perp Q \cosh(y_2 + \delta y_q), \quad (16)$$

$$\delta y_q = \ln(Q/q^+). \quad (17)$$

respectively. Finally, the Bjorken variable x_B might be evaluated using the relation

$$x_B \approx \frac{Q^2 + \mathcal{M}_{12}^2}{Q^2 + W_{\gamma p}^2 - m_N^2} \approx \frac{Q^2}{2q^- P^+} + \frac{M_{1\perp}}{P^+} e^{-y_1} + \frac{M_{2\perp}}{P^+} e^{-y_2}. \quad (18)$$

The cross section of electroproduction is dominated by single-photon exchange between leptonic and hadronic parts, and for this reason might be represented as

$$\frac{d\sigma_{e p \rightarrow e M_1 M_2 p}}{d \ln x_B dQ^2 d\Omega_h} = \frac{\alpha_{\text{em}}}{\pi Q^2} \left[(1-y) \frac{d\sigma_{\gamma p \rightarrow M_1 M_2 p}^{(L)}}{d\Omega_h} \right. \\ \left. + \left(1-y + \frac{y^2}{2} \right) \frac{d\sigma_{\gamma p \rightarrow M_1 M_2 p}^{(T)}}{d\Omega_h} \right], \quad (19)$$

where y is the inelasticity (fraction of electron energy that passes to the virtual photon, which should not be confused with the rapidities y_1, y_2 of produced quarkonia); $d\Omega_h$ represents the phase volume of the produced quarkonia pair and will be specified below. In (19) we assumed that the incident protons and electrons are not polarized, and $d\sigma^{(T)}$, $d\sigma^{(L)}$ are the contributions of the transversely and longitudinally polarized virtual photons. While the former is expected to dominate for longitudinal photons, the latter might get pronounced contributions at large virtualities.

The photoproduction cross section is related to the amplitude via

$$d\sigma_{\gamma p \rightarrow M_1 M_2 p}^{(L,T)} = \frac{dy_1 dp_{1\perp}^2 dy_2 dp_{2\perp}^2 d\phi \left| \mathcal{A}_{\gamma p \rightarrow M_1 M_2 p}^{(L,T)} \right|^2}{4(2\pi)^4 \sqrt{(W^2 + Q^2 - m_N^2)^2 + 4Q^2 m_N^2}} \times \delta((q + P_1 - p_1 - p_2)^2 - m_N^2), \quad (20)$$

which allows us to integrate out the dependence on ϕ . The restriction $|\cos \phi_0| \leq 1$ imposes an additional constraint on possible $(y_1, p_{1\perp})$ and $(y_2, p_{2\perp})$ values, at fixed photon-proton energy. In Fig. 1, we illustrate the typical kinematically allowed region for a fixed choice of E_γ , E_p , in EIC kinematics, as a function of rapidities and transverse momenta of quarkonia. At very high energies $P^+, q^- \gg M_{1,2}$, the domain turns into a narrow strip surrounding the curve (10) and has a typical width $\sim 1/P^+$. In this regime, the longitudinal momentum of the projectile remains almost constant, so it corresponds to the kinematics $x_B \sim \xi \ll 1$, which is outside the scope of our study. The color of each point in Fig. 1 illustrates the value of the invariant mass \mathcal{M}_{12} of the quarkonia pair. As we will show below, the dominant contribution to the cross section comes from the region $|t|_{\min} \lesssim |t| \lesssim 1 \text{ GeV}^2$; for this reason, we have also shown the line $t = -1 \text{ GeV}^2$ (the line $t = t_{\min}$ corresponds to the upper border of each colored domain). The observed anticorrelation between $|t|$ and \mathcal{M}_{12} might be understood if we take into account that, for fixed-energy of the quarkonia pairs, the variable $|t|$ reaches its minimum (and \mathcal{M}_{12} reaches its maximum) for quarkonia moving in *opposite* directions; vice versa, quarkonia moving in the *same* direction, will minimize \mathcal{M}_{12} but maximize $|t|$. In the experiment, due to finite resolution in the measurement of the photon energy W and the quarkonia kinematics $(y_{1,2}, p_{1,2})$, the narrow domains shown in Fig. 1 will get smeared. Because of this, the

where the δ function guarantees on shellness of the recoil proton. Taking into account that the vectors q, P_1 do not have transverse momenta, we may rewrite the argument of the δ function as

$$\begin{aligned} & (q + P_1 - p_1 - p_2)^2 - m_N^2 \\ &= \left(q + P_1 - p_1^\parallel - p_2^\parallel \right)^2 - (\mathbf{p}_1^\perp + \mathbf{p}_2^\perp)^2 - m_N^2 \\ &= \left(q + P_1 - p_1^\parallel - p_2^\parallel \right)^2 - ((p_1^\perp)^2 + (p_2^\perp)^2 \\ &\quad + 2p_1^\perp p_2^\perp \cos \phi) - m_N^2, \end{aligned} \quad (21)$$

where ϕ is the azimuthal angle between the transverse momenta of quarkonia $\mathbf{p}_1^\perp, \mathbf{p}_2^\perp$. We may rewrite the δ function in (20) as

$$\delta((q + P_1 - p_1 - p_2)^2 - m_N^2) = \frac{\delta(\phi - \phi_0)}{2p_{1\perp} p_{2\perp} |\sin \phi_0|}, \quad (22)$$

$$\phi_0 = \arccos \left[\frac{\left(q + P_1 - p_1^\parallel - p_2^\parallel \right)^2 - ((p_1^\perp)^2 + (p_2^\perp)^2 + m_N^2)}{2p_1^\perp p_2^\perp} \right], \quad (23)$$

values of \mathcal{M}_{12}^2 and t are not uniquely defined, but rather are distributed in some interval. The size of this effect depends crucially on the experimental setup, so we will not discuss it here with more detail. However, for any reasonably narrow bins in rapidity (Δy) or transverse momenta (Δp_\perp), the variables $y_{1,2}, p_{1,2}$ remain restricted to some finite domain.

In electroproduction experiments, instead of conventional fixing of the photon energy, it might be easier to treat the quarkonia variables $(y_1, p_{1\perp}, y_2, p_{2\perp}, \phi)$ as independent variables and express the photon energy in terms of these variables. The δ function in (20) can be rewritten as

$$\begin{aligned} & \delta((q + P_1 - p_1 - p_2)^2 - m_N^2) \\ &= \delta(W^2 + \mathcal{M}_{12}^2 - 2(q + P_1) \cdot (p_1 + p_2) - m_N^2) \\ &= \frac{\delta(W - W_0) + \delta(W + W_0)}{2W_0}, \end{aligned} \quad (24)$$

$$\begin{aligned} W_0^2 &= 2(q + P_1) \cdot (p_1 + p_2) + m_N^2 - \mathcal{M}_{12}^2 \\ &= \left(q^- + \frac{m_N^2}{2P^+} \right) \cdot (M_1^\perp e^{-y_1} + M_2^\perp e^{-y_2}) \\ &\quad + 2 \left(P^+ - \frac{Q^2}{2q^-} \right) \cdot (M_1^\perp e^{y_1} + M_2^\perp e^{y_2}) + m_N^2 - \mathcal{M}_{12}^2, \end{aligned} \quad (25)$$

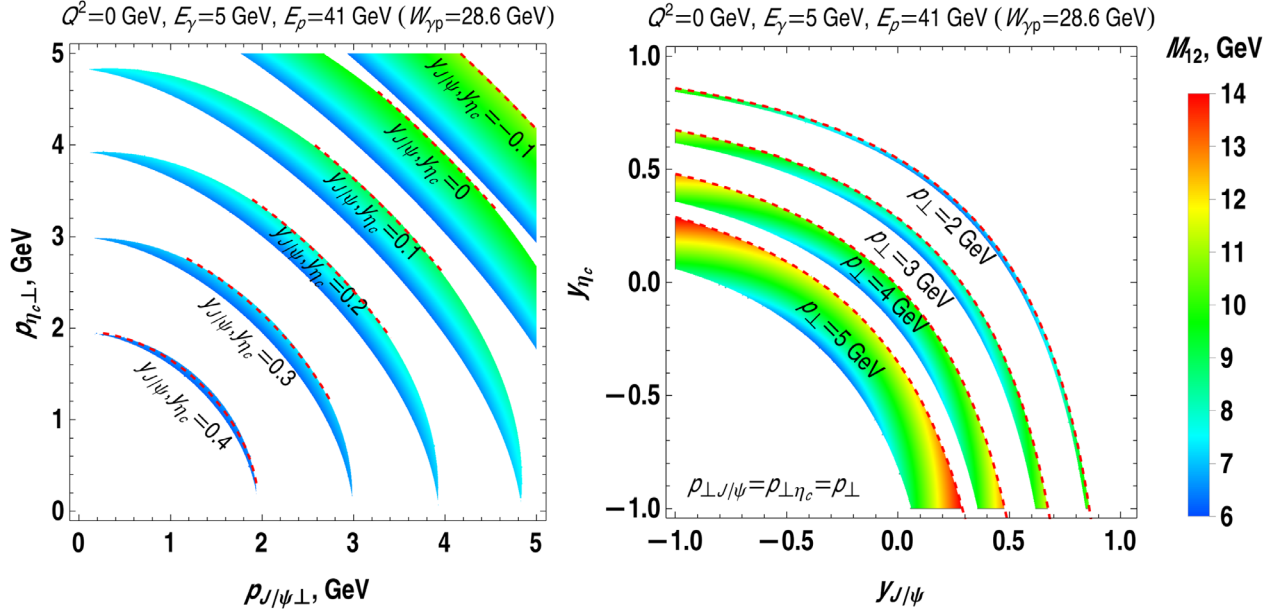


FIG. 1. The colored bands represent kinematically allowed regions for quarkonia pair production at fixed photon energy E_γ , virtuality Q^2 , and proton energy E_p . The left plot illustrates the allowed values of transverse momenta for different fixed rapidities $y_{1,2} \equiv y_{J/\psi}, y_{\eta_c}$ of both quarkonia. An increase of rapidities of both quarkonia leads to higher longitudinal components of their momenta and thus, in view of energy conservation, leads to smaller transverse momenta of quarkonia. The right plot illustrates the allowed values of rapidities at different fixed transverse momenta $|\mathbf{p}_{1,2}| \equiv p_{J/\psi}, p_{\eta_c}$. Akin to the left plot, in view of energy conservation, bands with smaller p_\perp require larger longitudinal components of both quarkonia, which translates into higher quarkonia rapidities. In both plots the color of each point encodes the value of the invariant mass \mathcal{M}_{12} of the quarkonia pair, as given in the color bar legend on the right side. The red dashed line inside each band corresponds to fixed momentum transfer to the proton $t = \Delta^2 = -1 \text{ GeV}^2$ (see the text for more explanation).

and q^- can be fixed from (11). After integration over all possible energies W (equivalent to integration over all possible x_B), we get for the electroproduction cross section

$$\frac{d\sigma_{ep \rightarrow eM_1M_2p}}{dQ^2 d\Omega_h} = \frac{\alpha_{\text{em}}}{4\pi Q^2} \left[(1-y) \frac{d\bar{\sigma}_{\gamma p \rightarrow M_1M_2p}^{(L)}}{d\Omega_h} + \left(1-y + \frac{y^2}{2}\right) \frac{d\bar{\sigma}_{\gamma p \rightarrow M_1M_2p}^{(T)}}{d\Omega_h} \right], \quad (26)$$

$$d\bar{\sigma}_{\gamma p \rightarrow M_1M_2p}^{(L,T)} = \frac{dy_1 dp_{1\perp}^2 dy_2 dp_{2\perp}^2 d\phi |\mathcal{A}_{\gamma p \rightarrow M_1M_2p}^{(L,T)}|^2}{4(2\pi)^4 W_0^2 \sqrt{(W_0^2 + Q^2 - m_N^2)^2 + 4Q^2 m_N^2}}, \quad (27)$$

where now $(y_1, p_{1\perp}, y_2, p_{2\perp}, \phi)$ are independent variables, and $d\bar{\sigma}_{\gamma p \rightarrow M_1M_2p}^{(L,T)}$ corresponds to the photoproduction cross section with the photon's energy evaluated using (10).

B. Amplitudes of the meson pair production process

For the evaluation of the amplitudes $\mathcal{A}_{\gamma p \rightarrow M_1M_2p}^{(L,T)}$, we will use the collinear factorization framework, which allows us

to express the amplitude in terms of the target GPDs [1–6]. We will assume that both the photon virtuality Q^2 and the quark mass m_Q are large parameters and also disregard the transverse momenta $\mathbf{\Delta}_\perp, \mathbf{p}_{a\perp}$ in the coefficient function. Furthermore, we will assume that the quarkonia pairs are always produced with sufficiently large relative momentum

$$p_{\text{rel}} \approx \frac{(2m_Q)v_{\text{rel}}}{\sqrt{1-v_{\text{rel}}^2}} \gtrsim \alpha_s(m_Q)m_Q, \\ v_{\text{rel}} = \sqrt{1 - \frac{p_1^2 p_2^2}{(p_1 \cdot p_2)^2}} \\ = \sqrt{1 - \frac{4M_1^2 M_2^2}{(\mathcal{M}_{12}^2 - M_1^2 - M_2^2)^2}}, \quad (28)$$

both with respect to each other, as well as with respect to recoil proton, to avoid potential factorization breaking by the exchange of soft gluons in the final state. We expect that the factorization should remain valid both in the Bjorken and in the photoproduction regimes.

The GPDs are conventionally defined in the symmetric frame specified in Appendix A, so for the coefficient functions evaluation we will temporarily switch to that

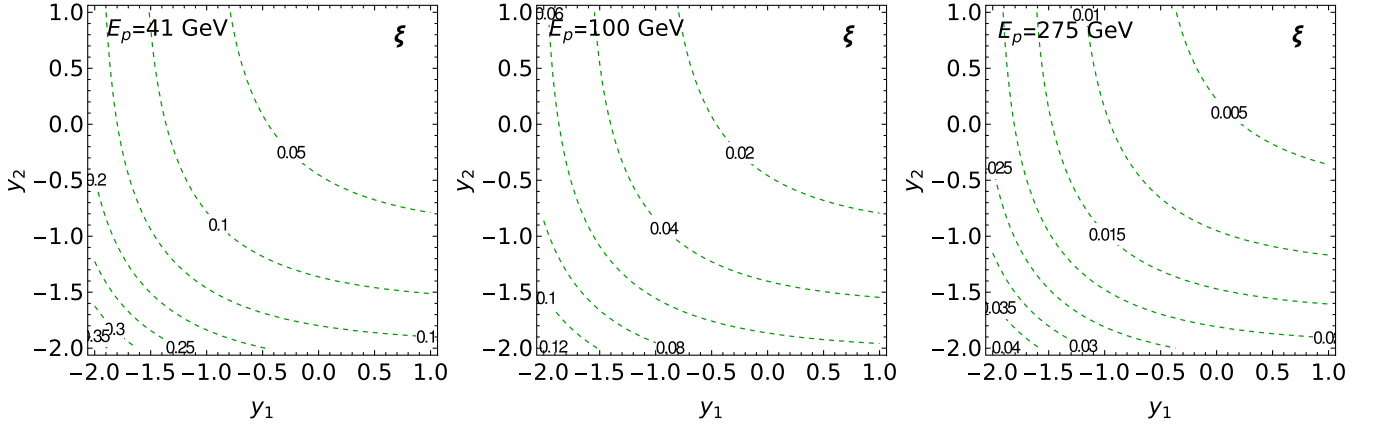


FIG. 2. The contour plot illustrates the relation of the skewedness variable $\xi = -(P_f^+ - P_i^+)/ (P_f^+ + P_i^+)$ to the rest-frame quarkonia rapidities y_1, y_2 , for different proton energies E_p , in EIC kinematics. For the sake of simplicity, we consider $J/\psi\eta_c$ production in the kinematics with zero transverse momenta and zero photon virtuality Q , which gives the dominant contribution to the total cross section. Labels on contour lines stand for the values of ξ .

frame.² In this frame, the momenta of the active parton (gluon), before and after interaction, are given explicitly by

$$\begin{aligned} k_i &= \left((x + \xi)\bar{P}^+, 0, -\frac{\Delta_\perp}{2} \right), \\ k_f &= \left((x - \xi)\bar{P}^+, 0, \frac{\Delta_\perp}{2} \right), \end{aligned} \quad (29)$$

where x is the light-cone fraction of average momentum, $x = (k_i^+ + k_f^+)/2\bar{P}^+$, and the skewedness variable ξ is related to x_B defined in (18) via the relations [3]

$$\xi = -\frac{\Delta_\perp^+}{2\bar{P}^+} = \frac{x_B}{2 - x_B}, \quad x_B = \frac{2\xi}{1 + \xi}. \quad (30)$$

In exclusive photoproduction, due to relation (18) it is possible to express ξ in terms of the produced quarkonia momenta. In Fig. 2, we illustrate the relation of the variable ξ to the rapidities y_1, y_2 of the quarkonia in the reference frame introduced in Sec. II A.

In Bjorken kinematics, the leading-order contribution to the amplitudes of quarkonia production comes from the gluon GPDs. The contributions of the light quark GPDs appear only via higher-order loop corrections and thus will be omitted in what follows. Furthermore, we will disregard the contributions of the transversity gluon GPDs H_T^g, E_T^g ,

²We need to mention that, in early studies [2,3,75,76], the GPDs were defined in an asymmetric frame, in which the momentum transfer of the incident photon is zero. Up to a trivial longitudinal boost, this frame essentially coincides with the frame introduced in Sec. II A. It is possible to relate the GPDs defined in different frames using some transformation of the arguments. However, since this frame is not widely used in the recent literature dedicated to GPD properties, we abstain from using it in what follows.

$\tilde{H}_T^g, \tilde{E}_T^g$, since at present there is no phenomenological parametrizations for these GPDs, and existing experimental bounds suggest that they should be negligibly small (see, e.g., explanation in [10,80]). By their definition, the transversity GPDs appear in the amplitudes multiplied by the momentum transfer to the proton Δ , which is small in the kinematics of interest, so we expect that their omission should be numerically justified. The contribution of the chiral even GPDs to the square of amplitude is given by

$$\begin{aligned} \sum_{\text{spins}} \left| \mathcal{A}_{\gamma p \rightarrow M_1 M_2 p}^{(\mathbf{a})} \right|^2 &= \frac{1}{(2 - x_B)^2} \left[4(1 - x_B)(\mathcal{H}_\mathbf{a}\mathcal{H}_\mathbf{a}^* + \tilde{\mathcal{H}}_\mathbf{a}\tilde{\mathcal{H}}_\mathbf{a}^*) \right. \\ &\quad - x_B^2(\mathcal{H}_\mathbf{a}\mathcal{E}_\mathbf{a}^* + \mathcal{E}_\mathbf{a}\mathcal{H}_\mathbf{a}^* + \tilde{\mathcal{H}}_\mathbf{a}\tilde{\mathcal{E}}_\mathbf{a}^* + \tilde{\mathcal{E}}_\mathbf{a}\tilde{\mathcal{H}}_\mathbf{a}^*) \\ &\quad - \left(x_B^2 + (2 - x_B)^2 \frac{t}{4m_N^2} \right) \mathcal{E}_\mathbf{a}\mathcal{E}_\mathbf{a}^* \\ &\quad \left. - x_B^2 \frac{t}{4m_N^2} \tilde{\mathcal{E}}_\mathbf{a}\tilde{\mathcal{E}}_\mathbf{a}^* \right], \quad \mathbf{a} = L, T, \end{aligned} \quad (31)$$

where the index \mathbf{a} refers to longitudinal or transverse photons, and, inspired by similar analysis of Compton scattering and single-meson deeply virtual production [81,82], we introduced the double-meson form factors

$$\begin{aligned} \mathcal{H}_\mathbf{a}(y_1, y_2, t) &= \int_{-1}^1 dx c_\mathbf{a}(x, y_1, y_2) H_g(x, \xi, t), \\ \mathcal{E}_\mathbf{a}(y_1, y_2, t) &= \int_{-1}^1 dx c_\mathbf{a}(x, y_1, y_2) E_g(x, \xi, t), \end{aligned} \quad (32)$$

$$\begin{aligned} \tilde{\mathcal{H}}_\mathbf{a}(y_1, y_2, t) &= \int_{-1}^1 dx \tilde{c}_\mathbf{a}(x, y_1, y_2) \tilde{H}_g(x, \xi, t), \\ \tilde{\mathcal{E}}_\mathbf{a}(y_1, y_2, t) &= \int_{-1}^1 dx \tilde{c}_\mathbf{a}(x, y_1, y_2) \tilde{E}_g(x, \xi, t), \end{aligned} \quad (33)$$

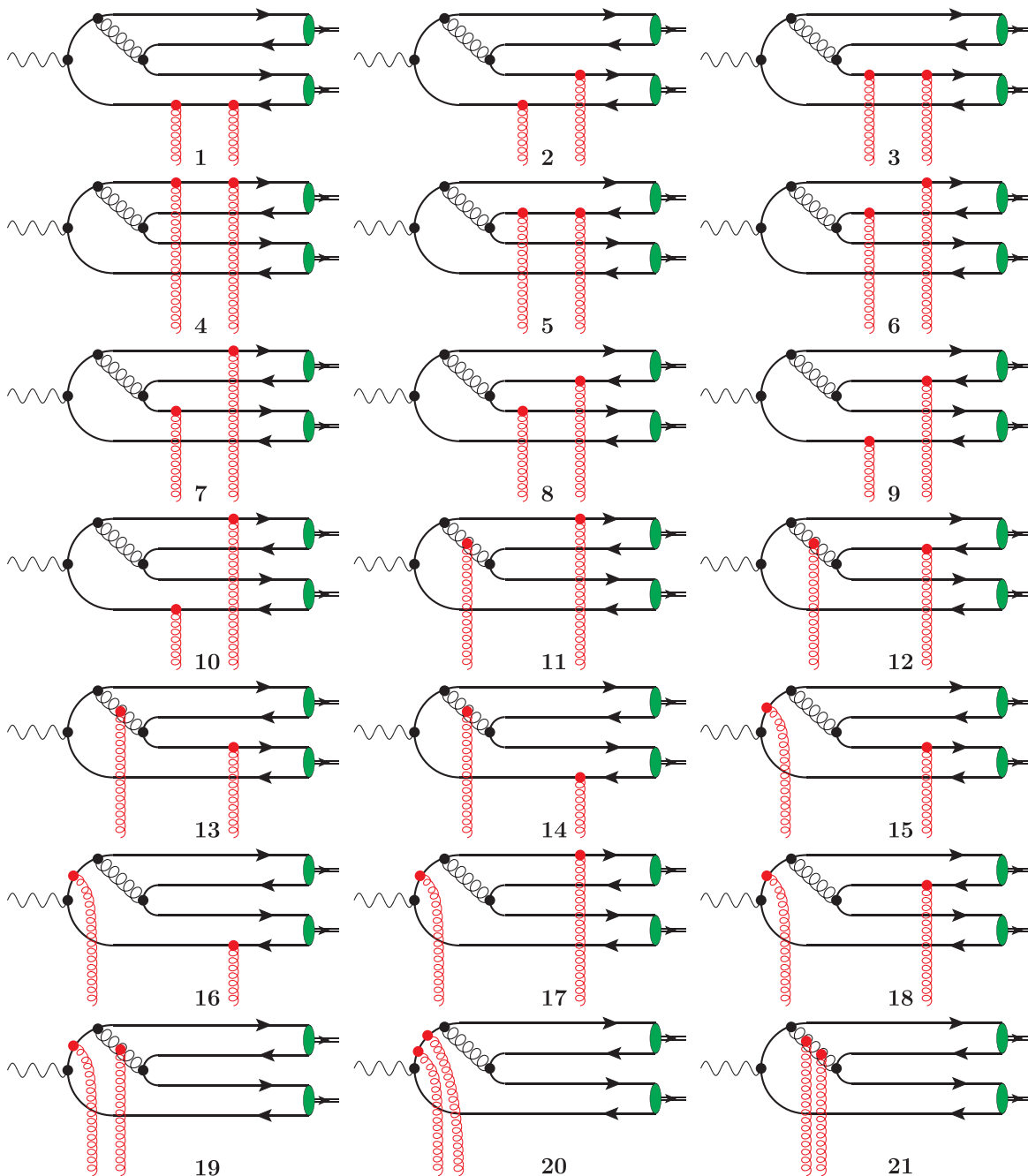


FIG. 3. Schematic illustration of the single quark loop (“type-A”) diagrams that contribute to the meson pair production. In all plots it is implied inclusion of diagrams that might be obtained by inversion of heavy quark lines (charge conjugation).

where the variable ξ should be understood as a function of y_1, y_2 , as defined in (30). The corresponding partonic amplitudes c_a, \tilde{c}_a might be evaluated perturbatively, taking into account the diagrams shown in Figs. 3 and 4. Since we assume that produced quarkonia are well separated from each other kinematically, the final Fock state of the system is a direct product of Fock states of individual quarkonia, and thus it is possible to express the amplitudes c_a, \tilde{c}_a in terms of the objects that encode the nonperturbative structure of individual quarkonia. This structure might be described in

terms of the nonperturbative long-distance matrix elements (LDMEs) of NRQCD [28–39] or, alternatively, in terms of light-cone distribution amplitudes (LCDAs). The equivalence of the two approaches has been discussed in detail in [83–85]. For the sake of definiteness, in what follows we will use the NRQCD approach for our evaluations. We briefly summarize the relation of this picture with the description in terms of LCDAs in Appendix B.

In the heavy quark limit, the relative velocity of heavy quarks inside the quarkonia is suppressed as $\sim \alpha_s(m_Q) \ll 1$,

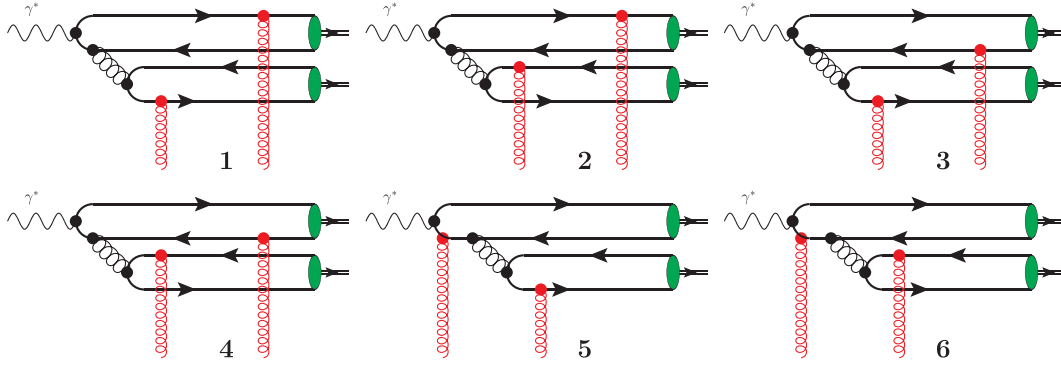


FIG. 4. Schematic illustration of the double quark loop (“type-B”) diagrams that contribute to the meson pair production. In all plots it is implied inclusion of diagrams that might be obtained by inversion of heavy quark lines (charge conjugation) in the first loop; diagrams 2, 4, 6 are related to diagrams 1, 3, 5 by charge conjugation (symmetry $z_2 \rightarrow 1 - z_2$).

and for this reason both heavy quarks inside each quarkonia carry approximately half of its momentum. Furthermore, according to NRQCD, for the evaluation of the functions c_a , \tilde{c}_a , we should project the final-state quark-antiquark pairs onto the states with definite quantum numbers, multiplying them by appropriate LDMEs. For this reason, we expect that these functions can be represented as

$$\begin{aligned} c_a(x, y_1, y_2) &= \sum_{ij} C_a^{(ij)}(x, y_1, y_2), \\ \tilde{c}_a(x, y_1, y_2) &= \sum_{ij} \tilde{C}_a^{(ij)}(x, y_1, y_2), \end{aligned} \quad (34)$$

where summation is done over different possible quantum numbers i, j of $Q\bar{Q}$ pairs inside both quarkonia. According to both NRQCD and potential models, the dominant Fock state in charmonium is the color singlet $\bar{c}c$ pair in the ${}^3S_1^{[1]}$ state for J/ψ , and the ${}^1S_0^{[1]}$ state for η_c , so we expect that the sums (34) might be approximated as

$$c_a(x, y_1, y_2) \approx C_a^{({}^3S_1^{[1]}, {}^1S_0^{[1]})}(x, y_1, y_2) \equiv C_a(x, y_1, y_2), \quad (35)$$

$$\tilde{c}_a(x, y_1, y_2) \approx \tilde{C}_a^{({}^3S_1^{[1]}, {}^1S_0^{[1]})}(x, y_1, y_2) \equiv \tilde{C}_a(x, y_1, y_2), \quad (36)$$

where at the last step in both equations we introduced a simplified notation without explicit quantum numbers. These functions C_a , \tilde{C}_a might be evaluated in perturbative QCD. Assuming equal sharing of quarkonium momentum between constituent quarks, it is possible to show that the typical virtuality of the gluon connecting different heavy lines is parametrically of order $\sim M_{12}^2/4$ for the diagrams in Fig. 3 and of order $\sim \min(M_1^2, M_2^2)$ for the diagrams in Fig. 4. This justifies the applicability of perturbation theory for evaluation of C_a , \tilde{C}_a , even for the diagrams that include three-gluon vertices in Fig. 3. The full expressions for the amplitudes and some technical details of its evaluation are provided in Appendix C.

The contribution of longitudinal photons to C_a vanishes in the limit of small $p_{a\perp} \ll M, Q$ in view of combined Lorentz and P parity. The contributions of the longitudinal photons to \tilde{C}_a do not vanish in this limit, although in the cross section it appears in convolution with numerically small helicity flip gluon GPDs \tilde{H}_g, \tilde{E}_g . Since for quasireal photons the contribution of longitudinal photons is suppressed by a factor Q/m_Q , we will disregard it altogether in the total (unpolarized) cross section.

The dependence on the variable x in the coefficient functions might be represented as a linear superposition of rational expressions

$$C_a(x, y_1, y_2) \sim \sum_{\ell} \frac{\mathcal{P}_{\ell}(x)}{\prod_{k=1}^{n_{\ell}} (x - x_k^{(\ell)} + i0)}, \quad (37)$$

where $\mathcal{P}_{\ell}(x)$ is a smooth polynomial of the variable x , and the denominator of each term in the sum (37) might include a polynomial with up to $n_{\ell} = 5$ nodes $x_k^{(\ell)}$ in the region of integration. The integral near the poles exists only in the principal value sense and is evaluated using

$$\frac{1}{x - x_k^{(\ell)} + i0} = \text{P.V.} \left(\frac{1}{x - x_k^{(\ell)}} \right) - i\pi\delta(x - x_k^{(\ell)}). \quad (38)$$

The position of the poles $x_k^{(\ell)}$ depends on all kinematic variables y_1, y_2, Q . In Fig. 5, we show the density plot that illustrates the behavior of the coefficient function $C_T(x, \xi, y_1, y_2)$ as a function of its arguments. While in the convolution integrals (32)–(33) we need to take the integral over all $x \in (-1, 1)$, we expect that a sizable contribution comes from the region near the poles of the coefficient function. From Fig. 5, we can see that in the coefficient function there are several poles, whose location depends on the kinematics of produced quarkonia. For the special case $Q = 0$ and $y_1 = y_2$, it is possible to express the position of these poles in terms of the variable ξ as

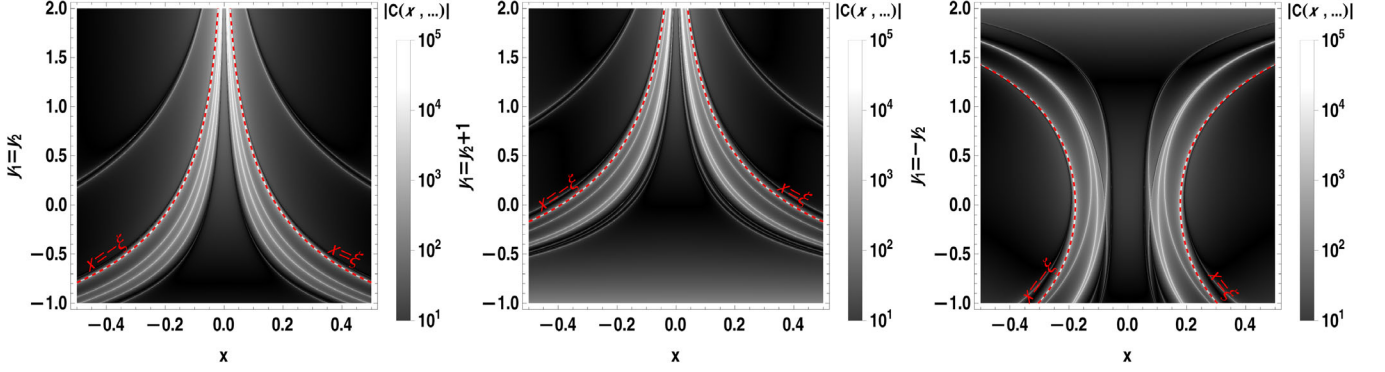


FIG. 5. Density plot which illustrates the coefficient function C_T (in relative units) as a function of the variables x and quarkonia rapidities y_1, y_2 . Left, central and right plots correspond to $y_1 = y_2$, $y_1 = y_2 + 1$ and $y_1 = -y_2$ respectively. Rapidities are taken in the reference frame introduced in Sec. II A, for proton energy $E_p^{(1)} = 41$ GeV; for other proton energies rapidities should be shifted by $\Delta y = \ln(E_p/E_p^{(1)})$. For the sake of definiteness, we considered the photoproduction regime ($Q = 0$) in all plots. White lines effectively demonstrate the position of the poles x_k^c of the coefficient function (37). For reference, we marked with red dashed lines the poles which correspond to $x = \pm\xi$, where the skewedness $\xi = \xi(y_1, y_2)$ was evaluated using (18), (30).

$$|x_k| = \left\{ \xi, \xi \left(1 - \frac{1}{1 + \xi} \right), \xi \left(1 - \frac{1}{2(1 + \xi)} \right), \xi \left(1 - \frac{2}{3(1 + \xi)} \right), \xi \left(1 - \frac{1}{3(1 + \xi)} \right), 3\xi \left(1 + \frac{1}{6(1 + \xi)} \right) \right\}. \quad (39)$$

Varying the rapidities y_1, y_2 of the observed quarkonia and virtuality Q^2 of the photon, it is possible to probe the gluon GPDs in the full kinematic range (x, ξ) . For this reason, the information about the gluon GPDs extracted from this process is complementary to what could be extracted from single quarkonia production or deeply virtual Compton scattering, which are mostly sensitive to gluon GPD near $x \approx \pm\xi$.

According to NRQCD [28–39], the color octet $\bar{Q}Q$ states might also contribute to quarkonia production, so the expression (31) should be generalized as

$$\sum_{\text{spins}} \left| \mathcal{A}_{\gamma p \rightarrow J/\psi \eta_c p}^{(a)} \right|^2 \approx \sum_{ij} \langle \mathcal{O}_i^{(J/\psi)} \rangle \langle \mathcal{O}_j^{(\eta_c)} \rangle \times \left| \mathcal{A}_{\gamma T p \rightarrow [\bar{Q}Q]_i [\bar{Q}Q]_j p} \right|^2, \quad (40)$$

where $\langle \mathcal{O}_i^{(M)} \rangle$ are the nonperturbative color singlet and octet LDMEs corresponding to a given state i of the $\bar{Q}Q$. In the heavy quark mass limit, the series (40) is expected to converge rapidly, so for numerical evaluations usually only the first few terms are relevant. As mentioned earlier, the dominant color singlet contribution is controlled by the LDMEs $\langle \mathcal{O}_{J/\psi}({}^3S_1^{[a]}) \rangle$, $\langle \mathcal{O}_{\eta_c}({}^1S_0^{[a]}) \rangle$, which according to phenomenological estimates have comparable values [86]

$$\langle \mathcal{O}_{J/\psi}({}^3S_1^{[a]}) \rangle \approx \langle \mathcal{O}_{\eta_c}({}^1S_0^{[a]}) \rangle \approx 0.3 \text{ GeV}^3. \quad (41)$$

The evaluation of the color octet amplitudes $\mathcal{A}_{\gamma T p \rightarrow [\bar{Q}Q]_8 [\bar{Q}Q]_8 p}$ is very similar to the color singlet case and differs only due to

different choice of the spin-color projections. However, according to phenomenological estimates, the color octet LDMEs of J/ψ mesons are very small [38],

$$\langle \mathcal{O}_{J/\psi}({}^3S_1^{[8]}) \rangle \approx 2.32 \times 10^{-4} \text{ GeV}^3, \quad (42)$$

$$\langle \mathcal{O}_{J/\psi}({}^1S_0^{[8]}) \rangle \approx 8.35 \times 10^{-3} \text{ GeV}^3, \quad (43)$$

$$\langle \mathcal{O}_{J/\psi}({}^3P_0^{[8]}) \rangle \approx 0, \quad (44)$$

and the color octet LDMEs of the η_c should be of the same order in view of the heavy quark mass limit relations [28]

$$\langle \mathcal{O}_{\eta_c}({}^1S_0^{[a]}) \rangle = \frac{1}{3} \langle \mathcal{O}_{J/\psi}({}^3S_1^{[a]}) \rangle, \quad a = 1, 8, \quad (45)$$

$$\langle \mathcal{O}_{\eta_c}({}^3S_1^{[8]}) \rangle = \langle \mathcal{O}_{J/\psi}({}^1S_0^{[8]}) \rangle, \quad (46)$$

$$\langle \mathcal{O}_{\eta_c}({}^1P_1^{[8]}) \rangle = 3 \langle \mathcal{O}_{J/\psi}({}^3P_0^{[8]}) \rangle. \quad (47)$$

For this reason, in what follows we may safely omit the color octet contributions.³

³We need to mention that, at very large transverse momenta $p_T \gtrsim 5\text{--}10$ GeV, it is known that color octet contributions might give relevant contribution to inclusive quarkonia production [33,34,40]. However, in our evaluations, we do not consider such large values of p_T , since the exclusive cross section is strongly suppressed in that kinematics due to suppression of gluon GPDs at large $|t| \sim p_T^2$.

III. NUMERICAL RESULTS

For the sake of definiteness, for our predictions we use the Kroll-Goloskokov parametrization of the gluon GPDs [80,87–91]. This parametrization effectively takes into account the evolution of the gluon distributions, introducing a mild dependence of the model parameters on the factorization scale μ_F . In what follows, for the sake of definiteness, we will choose the scale $\mu_F = \mu_R \approx \sqrt{M_{J/\psi}^2 + Q^2}$, which interpolates smoothly between $\mu_F \approx M_{J/\psi}$ in the photoproduction regime and $\mu_F \approx Q$ in the Bjorken regime. In Fig. 6, we show the dependence of the typical cross section on the choice of this factorization scale. We may observe that this dependence is mild at

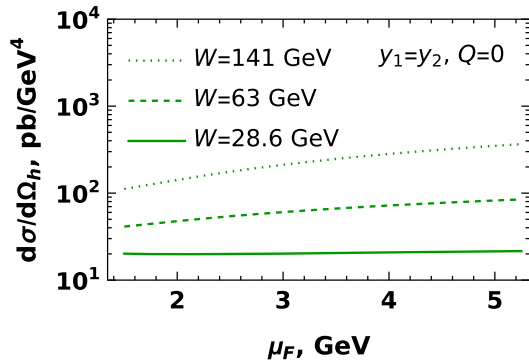


FIG. 6. Dependence of the cross section on the choice of factorization scale μ_F . The frame label $d\sigma/d\Omega_h$ on the vertical axis is a shorthand notation for $d\sigma/dy_1 dp_1^2 dy_2 dp_2^2 d\phi$. Chosen values of W correspond to photon-proton energies $E_\gamma \times E_p = 18 \times 275$, 100×10 , and 5×41 GeV respectively. In the photoproduction regime, these values of W correspond to values of the Bjorken variable $x_B \approx 1.9 \times 10^{-3}$, 9.4×10^{-3} , and 4.5×10^{-2} , respectively. All frame-dependent variables are given in the reference frame described in Sec. II A.

moderate energies, but becomes very pronounced at very high energies (small x_B). Such behavior is not surprising: it is known from studies of *single* quarkonia photoproduction [40–43] that this dependence is due to omitted loop corrections, and these corrections become especially pronounced in the small- x_B kinematics.

We would like to start the presentation of results with a discussion of the cross section (27) dependence on the virtuality Q , shown schematically in Fig. 7. This dependence is very mild in the photoproduction regime ($Q \lesssim M_{J/\psi}$), since the hard scale in this kinematics is controlled by the quarkonium mass. In the Bjorken regime ($Q \gg M_{J/\psi}$), the virtuality Q plays the role of the hard scale, which leads to a pronounced dependence on Q . We can see that the cross section is strongly suppressed, so the experimental studies of this regime become very challenging. For small $Q \lesssim M_{J/\psi}$, the cross section is dominated by the transversely polarized J/ψ mesons, similar to single J/ψ production. This contribution is sensitive to the gluon GPDs H_g , E_g . The contribution of the longitudinally polarized J/ψ mesons is controlled by the helicity flip gluon GPDs \tilde{H}_g , \tilde{E}_g , which are less known phenomenologically, although they are clearly significantly smaller than the unpolarized GPDs. We also observe that the GPDs H_g , E_g might contribute to longitudinally polarized photons via $\sim \mathcal{O}(\mathbf{p}_{\perp J/\psi})$ corrections, although a systematic analysis of this contribution would also require us to take into account currently unknown twist-three gluon GPDs. In view of these uncertainties, we abstain from making predictions for the longitudinal polarization.

In Fig. 8, we show the dependence of the cross section (27) on the transverse momenta $\mathbf{p}_{1\perp}$, $\mathbf{p}_{2\perp}$. In the collinear factorization approach, this dependence is largely due to the gluon GPD dependence on the invariant momentum transfer t (8): most of the phenomenological models implement a pronounced (nearly exponential)

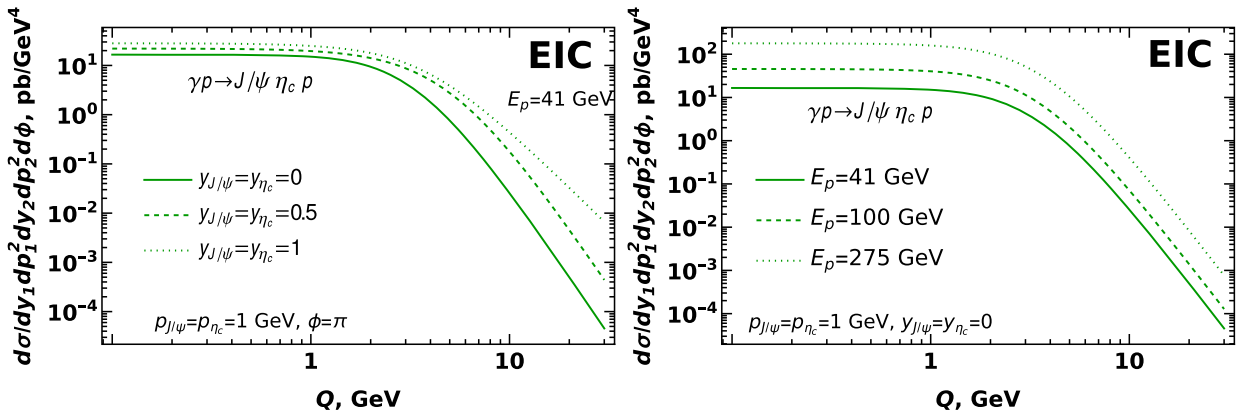


FIG. 7. Dependence of the photoproduction cross section (27) on the virtuality Q of the photon. On the left and right, we compare predictions for different rapidities $y_{J/\psi}, y_{\eta_c}$ and different proton energies E_p . Both plots clearly illustrate the transition from photoproduction to Bjorken regime in the region $Q \sim 1-2M_{J/\psi}$. In both plots, the photon energy is evaluated from (1) and (11). All frame-dependent variables are given in the reference frame described in Sec. II A.

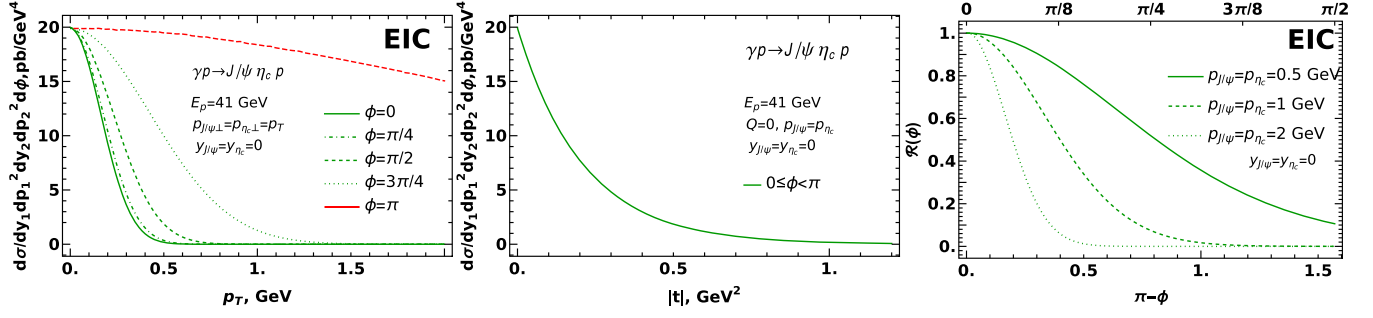


FIG. 8. Dependence of the photoproduction cross section (27) on the transverse momenta p_T of the quarkonia (left), invariant momentum transfer t to the proton (center), and the angle ϕ between the quarkonia (right). Since the cross sections at different p_T differ quite significantly, in order to facilitate the comparison of their ϕ dependence, in the right plot we normalized them to unity in the maximum (angle $\phi = \pi$). For the sake of definiteness, we considered the case of photoproduction ($Q = 0$) at central rapidities ($y_1 = y_2 = 0$) in the frame described in Sec. II A; for other virtualities and rapidities, the p_T and ϕ dependence have very similar shapes. All frame-dependent variables are given in the reference frame described in Sec. II A.

behavior at small t . At large angles $\phi \approx \pi$ between transverse momenta of quarkonia (back-to-back kinematics), the cross section has a sharp peak, which might be understood from the definition (8): this point minimizes $|t|$ at fixed $|p_{1\perp}|, |p_{2\perp}|$. As discussed in Sec. II A, the transverse momenta $p_{1\perp}, p_{2\perp}$ also appear in other observables (e.g., via kinematic constraints, “transverse” masses $M_{1,2}^\perp$) and thus a mild p_T dependence exists even for $p_{1\perp} = -p_{2\perp}$, as could be seen from the long red dashed line in the left panel of Fig. 8. Since in the collinear approach we neglected the p_T dependence in the coefficient functions, the results are valid only for small $p_T \ll \max(Q, m_Q)$; in the opposite limit (wide angle scattering kinematics), the cross section will be strongly suppressed as a function of the variable p_T even for $p_T = p_{1\perp} = -p_{2\perp}$. The central panel in Fig. 8 clearly demonstrates that, for any fixed $\phi \neq \pi$, the cross section has the same dependence on invariant momentum transfer t . This happens because in collinear approach we disregard the transverse momenta in evaluation of the coefficient function, so ϕ dependence exists only due to t dependence of the gluon GPDs. In Fig. 9, we illustrate the uncertainty of these cross sections due to choice of the scale μ_F , varying it in the range

$\mu_F \in (M_{J/\psi}/2, 2M_{J/\psi})$. As discussed earlier, this uncertainty is very moderate at low energies, yet becomes very pronounced (up to a factor of 2) at high energies. This indicates that loop corrections might give pronounced contribution in that kinematics.

In Fig. 10, we show the dependence of the p_T -integrated cross section on the rapidities of the produced quarkonia. In the left panel, we show the dependence of the cross section on the average rapidity $y_1 = y_2$. As expected, the cross section grows with y due to the increase of photon energy W^2 , the corresponding decrease of x_B, ξ , and the growth of the gluon GPDs in that kinematics. In the right panel, we show the dependence on the rapidity difference Δy at central rapidities. The cross section decreases as a function of Δy , because the variables x_B, ξ , the longitudinal recoil to the proton, and the longitudinal momentum transfer $|t_{\min}|$ grow as a function of Δy at fixed $Y = (y_1 + y_2)/2$, and the amplitude decreases due to suppression of gluon GPDs with $|t|$. Finally, in Fig. 11, we show the distribution of the produced $J/\psi \eta_c$ pairs over their invariant mass \mathcal{M}_{12} . The distribution has a pronounced peak near $\mathcal{M}_{12} \approx 7$ GeV, which demonstrates that the quarkonia pairs predominantly are produced with a small relative momentum $\sim 2-3$ GeV.

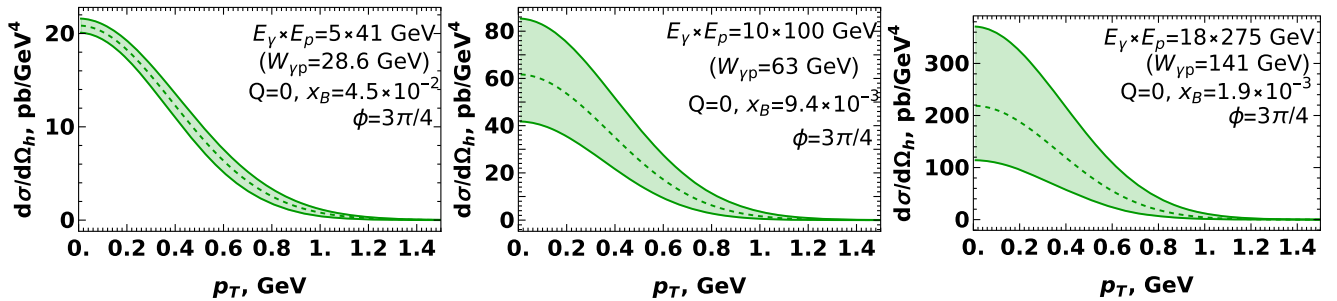


FIG. 9. Uncertainty of the cross section due to choice of factorization scale μ_F . In all plots, the central dashed line corresponds to $\mu_F = M_{J/\psi}$, whereas upper and lower limits of the colored bands correspond to $\mu_F = 2M_{J/\psi}$ and $\mu_F = M_{J/\psi}/2$, respectively. For the sake of definiteness, in all plots we considered that the angle between J/ψ and η_c is $\phi = 3\pi/4$; for other angles, the uncertainty due to choice of μ_F has the same magnitude.

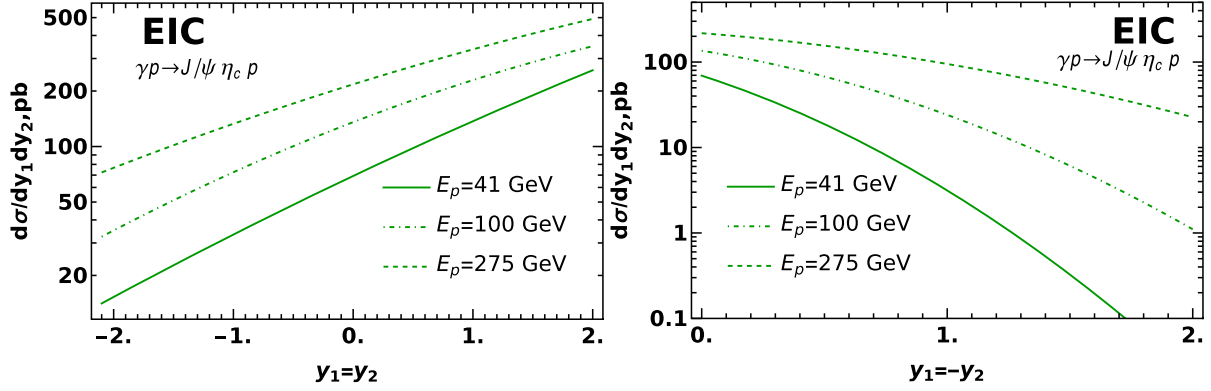


FIG. 10. Dependence of the cross section on the rapidities y_1, y_2 of the two quarkonia for several proton energies in EIC kinematics. Left: we illustrate the dependence on the average rapidity ($y_1 = y_2$). Right: we consider the dependence on the rapidity difference at central rapidities ($y_1 = -y_2 = \Delta y/2$).

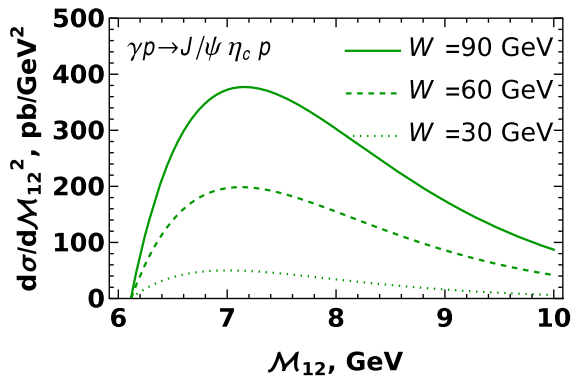


FIG. 11. Distribution of the produced quarkonia pairs over their invariant mass M_{12} for several fixed invariant energies W of the γp collision.

IV. CONCLUSIONS

In this paper, we studied, in the collinear factorization approach, the exclusive photoproduction of heavy charmonia pairs with opposite C parities ($J/\psi \eta_c$). In our analysis, we focused on the kinematics of moderate values of x_B , achievable with low-energy ep beams at the Electron Ion Collider. This regime corresponds to values of the Bjorken variable $x_B \in (10^{-3}, 10^{-1})$. We performed evaluations in leading order, assuming that higher-order corrections are suppressed at least as $\alpha_s(m_Q)$. We focused on the photoproduction regime ($Q^2 \approx 0$) and found that the dependence of the photoproduction cross section on the virtuality Q is quite mild up to $Q \lesssim m_Q \approx 1.2\text{--}1.5$ GeV. The cross section has a pronounced dependence on the invariant momentum transfer t and vanishes for $|t| \gtrsim 1$ GeV². This implies that the quarkonia pairs are produced predominantly in back-to-back kinematics (with oppositely directed transverse momenta), which minimizes $|t|$. The produced J/ψ mesons are predominantly transversely polarized, and the

amplitude of the process obtains the dominant contribution from the unpolarized gluon GPD H_g . The coefficient function (partonic amplitude) has several poles (in addition to the classical $x = \pm\xi$), whose positions depend on the kinematics of the produced quarkonia. In view of the complexity of the coefficient function, the deconvolution (direct extraction of GPDs from amplitudes) is apparently not possible. Nevertheless, we believe that the process might be useful to constrain existing models of phenomenological GPDs, especially outside the $x = \pm\xi$ line.

The results presented here complement our earlier analysis [65] done in the color dipole framework in the kinematics $x_B \ll 1$ and agrees with it by an order of magnitude if extended to the region of common validity (largest energy ep beams at EIC, small $x_B \ll 1$). However, the collinear factorization approach might be not reliable there due to large NLO corrections and onset of saturation effects.

Numerically, the evaluated cross sections are on par with similar estimates for $2 \rightarrow 3$ processes ($\gamma^* p \rightarrow \gamma M p$, $M = \pi, \rho$) suggested recently in the literature [12–21]. This happens because the emission of a photon in the final state leads to a suppression by the fine-structure constant α_{em} , on par with the suppression due to heavy quark mass in the production of heavy quarkonia pairs. For this reason, both $\gamma^* p \rightarrow \gamma M p$ and heavy quarkonia production could be used as complementary tools for the study of both quark and gluon GPDs.

ACKNOWLEDGMENTS

We thank our colleagues at UTFSM University for encouraging discussions. This research was partially supported by Proyecto ANID PIA/APOYO AFB180002 (Chile) and Fondecyt (Chile) Grants No. 1180232 and No. 1220242. Powered@NLHPC: This research was partially supported by the supercomputing infrastructure of the NLHPC (ECM-02).

APPENDIX A: SYMMETRIC FRAME

In the collinear factorization framework, the evaluations in Bjorken kinematics are frequently performed in the so-called symmetric frame [2,3,73,75–79], in which the vectors of photon momentum q and $\bar{P} = (P_i + P_f)/2$ (the average momentum of the target before and after collision) do not have transverse momenta. This frame differs from the reference frame introduced in Sec. II A by a transverse boost, supplemented by a rotation in the transverse plane [3]. In this paper, we focus on the kinematics of small transverse momenta Δ_\perp , which eventually will be disregarded during evaluations of the coefficient functions, so the parameters of the boost and rotation are also small, $\sim \Delta_\perp/P^+$, and will give only $\mathcal{O}(\Delta_\perp^2)$ corrections to \pm components of light-cone vectors. For this reason, in what follows, we will abuse notations and disregard possible differences of \pm components in these two frames.

Explicitly, the light-cone decomposition of photon and proton momenta is given by

$$q = \left(Z\bar{P}^+, -\frac{Q^2}{2Z\bar{P}^+}, \mathbf{0}_\perp \right), \quad (\text{A1})$$

$$\bar{P} = \frac{P_f + P_i}{2} = \left(\bar{P}^+, \frac{\bar{m}_N^2}{2\bar{P}^+}, \mathbf{0}_\perp \right), \quad \bar{m}_N^2 = m_N^2 - \frac{t}{4}, \quad (\text{A2})$$

$$\Delta = P_f - P_i = \left(-2\xi\bar{P}^+, \frac{\xi\bar{m}_N^2}{\bar{P}^+}, \Delta_\perp \right), \quad (\text{A3})$$

so the momenta of the proton before collision (P_i) and after collision (P_f) are given explicitly by

$$P_{f,i} = P \pm \frac{\Delta}{2} = \left((1 \mp \xi)\bar{P}^+, (1 \pm \xi)\frac{\bar{m}_N^2}{2\bar{P}^+}, \pm \frac{\Delta_\perp}{2} \right) \quad (\text{A4})$$

and the invariant momentum transfer to the proton is

$$t = \Delta^2 = -4\xi^2 \left(m_N^2 - \frac{t}{4} \right) - \Delta_\perp^2 = -\frac{4\xi^2 m_N^2 + \Delta_\perp^2}{1 - \xi^2}. \quad (\text{A5})$$

The variable \bar{P}^+ might be related to variables defined in Sec. II A as

$$\begin{aligned} \bar{P}^+ &= P^+ + \frac{q^+ - M_1^\perp e^{-y_1} - M_2^\perp e^{-y_2}}{2} \\ &= \frac{m_N^2}{2P^-} + \frac{q^+ - M_1^\perp e^{-y_1} - M_2^\perp e^{-y_2}}{2}. \end{aligned} \quad (\text{A6})$$

The variable Z might be fixed from conservation of plus components of momenta as

$$Z = \frac{q^+}{\bar{P}^+} = -2\xi + \frac{M_{1\perp}}{2\bar{P}^+} e^{-y_1} + \frac{M_{2\perp}}{2\bar{P}^+} e^{-y_2}. \quad (\text{A7})$$

APPENDIX B: RELATION OF QUARKONIA DISTRIBUTION AMPLITUDES AND NRQCD

In this appendix, for the sake of completeness, we discuss briefly the relation between the descriptions of quarkonia structure in terms of light-cone distribution amplitudes and NRQCD, summarizing the findings of [83–85]. The definitions of the spin-0 quarkonia distribution amplitudes are straightforward extensions of general results formulated for light quarks [92–96]. For the spinless η_c meson, at leading twist, there is only one distribution amplitude defined as

$$\begin{aligned} \Phi_{\eta_c}(z) &= \int \frac{d\eta}{2\pi} e^{izp^+\eta} \left\langle 0 \left| \bar{\psi} \left(-\frac{\eta}{2} \right) \gamma^+ \gamma_5 \mathcal{L} \left(-\frac{\eta}{2}, \frac{\eta}{2} \right) \right. \right. \\ &\quad \left. \left. \times \psi \left(\frac{\eta}{2} \right) \right| \eta_c(p) \right\rangle, \end{aligned} \quad (\text{B1})$$

$$\mathcal{L} \left(-\frac{\eta}{2}, \frac{\eta}{2} \right) \equiv \mathcal{P} \exp \left(i \int_{-\eta/2}^{\eta/2} d\zeta A^+(\zeta) \right), \quad (\text{B2})$$

where z is the fraction of the quarkonium momentum carried by the c quark, and \mathcal{L} is the standard path-ordered gauge link. The spin-1 J/ψ meson is characterized by two independent leading-twist distributions Φ_\parallel and Φ_\perp defined as

$$\begin{aligned} \Phi_{J/\psi}^\parallel(z) &= \int \frac{d\eta}{2\pi} e^{izp^+\eta} \left\langle 0 \left| \bar{\psi} \left(-\frac{\eta}{2} \right) \gamma^+ \mathcal{L} \left(-\frac{\eta}{2}, \frac{\eta}{2} \right) \right. \right. \\ &\quad \left. \left. \times \psi \left(\frac{\eta}{2} \right) \right| J/\psi(p) \right\rangle, \end{aligned} \quad (\text{B3})$$

$$\begin{aligned} \Phi_{J/\psi}^\perp(z) &= \int \frac{d\eta}{2\pi} e^{izp^+\eta} \left\langle 0 \left| \bar{\psi} \left(-\frac{\eta}{2} \right) (-i\sigma^{\mu\nu} \varepsilon_{J/\psi,\mu}^*(p)) \right. \right. \\ &\quad \left. \left. \times \mathcal{L} \left(-\frac{\eta}{2}, \frac{\eta}{2} \right) \psi \left(\frac{\eta}{2} \right) \right| J/\psi(p) \right\rangle, \end{aligned} \quad (\text{B4})$$

where it is assumed that the J/ψ meson moves in the plus direction, $\varepsilon_{J/\psi}(p)$ is the polarization vector of J/ψ mesons, and in (B4) the polarization vector $\varepsilon_{J/\psi}$ satisfies $n \cdot \varepsilon_{J/\psi} = p \cdot \varepsilon_{J/\psi,\mu}^*(p) = 0$. Sometimes the definitions (B1)–(B4) might include distribution amplitudes normalized to unity and, for this reason, might contain additional normalization factors (quarkonia decay constants) $f_{J/\psi}$, f_{η_c} . In what follows and up to the end of this section, for the sake of brevity, we will use a common notation Φ_M for the distribution amplitude of quarkonium state $|M(p)\rangle$ and f_M for the corresponding decay constant.

The complementary NRQCD approach constructs the description of quarkonia states M in terms of long-distance matrix elements with structure $\langle 0 | \hat{\mathcal{O}}_M | M(p) \rangle$, where $\hat{\mathcal{O}}_M$ is a set of *local* operators built from operators of quarks, antiquarks, and their covariant derivatives. The relation of

the two approaches has been discussed in detail in [83–85]. The distribution amplitudes might be expressed in terms of NRQCD LDMEs as

$$\Phi_M(z) = \hat{\Phi}_M(z) \frac{\langle 0 | \hat{\mathcal{O}}_M | M(p) \rangle}{2\sqrt{m_Q}} (1 + \mathcal{O}(v^2)), \quad (\text{B5})$$

where $\hat{\Phi}(z)$ is the perturbative (partonic-level) distribution amplitude, and the denominator is conventionally added to take into account the difference between normalizations of Fock states used in LCDA and NRQCD pictures. In the heavy quark mass limit, it is possible to make a systematic expansion over the velocities $v \sim \alpha_s(m_c) \ll 1$ of the quarks in the quarkonium rest frame, and in the leading order over v the distribution amplitude is simply given by

$$\hat{\Phi}_M(z) \sim f_M \delta\left(z - \frac{1}{2}\right) + \mathcal{O}(v^2). \quad (\text{B6})$$

Because of NLO corrections, the amplitude (B6) obtains nontrivial dependence on z , which might be found in [83]. We will eventually disregard this dependence, since formally it is a higher-order correction in α_s . Conversely, the color singlet long-distance matrix elements $\langle 0 | \hat{\mathcal{O}}_M | M(p) \rangle$ might be expressed in terms of the moments of the distribution amplitude $\Phi_M(z)$, thus demonstrating that it is possible to construct a correspondence between the two approaches.

Finally, we would like to discuss a modification of the expressions (34) when the finite width of z distribution is taken into account. In view of the expected dominance of the leading-twist distribution amplitudes, the functions c_a , \tilde{c}_a might be represented as

$$c_a(x, y_1, y_2) = \int dz_1 dz_2 C_a(x, z_1, z_2, y_1, y_2) \times \Phi_\eta(z_1) \Phi_{J/\psi}^{(a)}(z_2), \quad (\text{B7})$$

$$\tilde{c}_a(x, y_1, y_2) = \int dz_1 dz_2 \tilde{C}_a(x, z_1, z_2, y_1, y_2) \times \Phi_\eta(z_1) \Phi_{J/\psi}^{(a)}(z_2), \quad (\text{B8})$$

where $\Phi_{J/\psi}^{(a)}$ should be understood as $\Phi_{J/\psi}^{\parallel}$ for longitudinally polarized photons and as $\Phi_{J/\psi}^{\perp}$ for transverse photons. The evaluation of the functions $C_a(x, z_1, z_2, y_1, y_2)$, $\tilde{C}_a(x, z_1, z_2, y_1, y_2)$ might be done perturbatively and largely follows the same steps as similar evaluation in NRQCD (see Appendix C). From the Dirac structure of (B1)–(B4), we may deduce that the corresponding spin projectors for $\bar{Q}Q$ states onto η_c and J/ψ in leading twist are given by

$$\hat{P}_{\eta_c} = \frac{1}{4} \hat{P} \gamma_5, \quad \hat{P}_{J/\psi, \parallel} = \frac{1}{4} \hat{P}, \quad \hat{P}_{J/\psi, \perp} = \frac{1}{4} \hat{P} \hat{e}_{J/\psi}^*. \quad (\text{B9})$$

As we will see below, these expressions, up to mass terms (formally higher twist corrections), coincide with similar NRQCD projectors (C13) and (C14). Because of space limitations, we will not provide here the analytic expressions for $C_a(x, z_1, z_2, y_1, y_2)$, $\tilde{C}_a(x, z_1, z_2, y_1, y_2)$. In the approximation (B6), the integrals over z_1, z_2 in (B7) and (B8) may be evaluated analytically, so these expressions simplify as

$$c_a(x, y_1, y_2) \approx f_{J/\psi} f_{\eta_c} C_a\left(x, \frac{1}{2}, \frac{1}{2}, y_1, y_2\right) + \mathcal{O}(\alpha_s(m_c)), \quad (\text{B10})$$

$$\tilde{c}_a(x, y_1, y_2) \approx f_{J/\psi} f_{\eta_c} \tilde{C}_a\left(x, \frac{1}{2}, \frac{1}{2}, y_1, y_2\right) + \mathcal{O}(\alpha_s(m_c)), \quad (\text{B11})$$

where the decay constants $f_{J/\psi}^2$ and $f_{\eta_c}^2$ are proportional to the color singlet LDMEs $\langle \mathcal{O}_{J/\psi}^{[1]}({}^3S_1^{[a]}) \rangle$, $\langle \mathcal{O}_{\eta_c}^{[1]}({}^1S_0^{[a]}) \rangle$, respectively [40,62]. These results allow us to understand the relation of the functions $C_a(x, z_1, z_2, y_1, y_2)$, $\tilde{C}_a(x, z_1, z_2, y_1, y_2)$ with the NRQCD functions C_a , \tilde{C}_a from (35) and (36).

APPENDIX C: EVALUATION OF THE COEFFICIENT FUNCTIONS

The evaluation of the coefficient functions (partonic amplitudes) relies on standard light-cone rules formulated in [1,3,45,73,97,98]. We assume that both photon virtuality Q and the quark mass m_Q are large parameters, $Q \sim m_Q \sim \sqrt{s_{\gamma p}}$, tacitly disregarding the proton mass and momentum transfer to the proton t . As we discussed in Sec. II B, in the heavy quark mass limit it is possible to disregard internal motion of the quarks inside quarkonia, assuming that the momentum of the quarkonium is shared equally between the quarks, and disregard the difference of J/ψ and η_c masses, assuming $M_{J/\psi} \approx M_\eta \approx 2m_Q$. The evaluation of the partonic amplitudes requires computation of the Feynman diagrams shown in Figs. 3 and 4 and was done using the FeynCalc package for *Mathematica* [99,100]. This evaluation resembles similar studies of the single quarkonia photoproduction well known from the literature [40–43]. Below we provide some technical details that might help to understand the main steps and assumptions needed for derivation of the final result.

Since GPDs are conventionally defined in the symmetric frame, we perform evaluation of the coefficient function in that frame, assuming that all momenta might be related

using the transformations described in Appendix A. The momenta of partons (gluons) in this frame, before and after interaction, are given, respectively, by

$$k_{i,f} = \left((x \pm \xi) \bar{P}^+, 0, \mathbf{k}_\perp \mp \frac{\Delta_\perp}{2} \right). \quad (\text{C1})$$

Furthermore, to simplify further notations, we will shift the rapidities of quarkonia and rewrite their momenta as

$$p_a = \left(e^{\tilde{y}_a} \bar{P}^+, \frac{(M_a^\perp)^2 e^{-\tilde{y}_a}}{2\bar{P}^+}, \mathbf{p}_a^\perp \right), \quad a = 1, 2, \quad (\text{C2})$$

$$\tilde{y}_a = -y_a + \ln(M_a^\perp/2\bar{P}^+). \quad (\text{C3})$$

This modification allows us to suppress numerous factors $\sim M_a^\perp/\bar{P}^+$, so the coefficient functions will depend only on two independent dimensional variables, m_Q^2 and Q^2 . For example, the variable Z defined in (A7) will turn into a simple expression

$$Z = -2\xi + e^{\tilde{y}_1} + e^{\tilde{y}_2}. \quad (\text{C4})$$

Since we consider that formally both M_a and \bar{P}^+ are large parameters of the same order, the variables y_a and \tilde{y}_a are also of the same order, and thus switching from y_a to \tilde{y}_a does not require modification of the underlying counting rules.

The chiral even gluon GPDs, which are expected to give the dominant contributions, are defined as [3,40]

$$\begin{aligned} F^g(x, \xi, t) &= \frac{1}{\bar{P}^+} \int \frac{dz}{2\pi} e^{ix\bar{P}^+} \langle P' | G^{+\mu a} \left(-\frac{z}{2} n \right) \mathcal{L} \left(-\frac{z}{2}, \frac{z}{2} \right) G_\mu^{+a} \left(\frac{z}{2} n \right) | P \rangle \\ &= \left(\bar{U}(P') \gamma_+ U(P) H^g(x, \xi, t) + \bar{U}(P') \frac{i\sigma^{+\alpha} \Delta_\alpha}{2m_N} U(P) E^g(x, \xi, t) \right), \end{aligned} \quad (\text{C5})$$

$$\begin{aligned} \tilde{F}^g(x, \xi, t) &= \frac{-i}{\bar{P}^+} \int \frac{dz}{2\pi} e^{ix\bar{P}^+} \langle P' | G^{+\mu a} \left(-\frac{z}{2} n \right) \mathcal{L} \left(-\frac{z}{2}, \frac{z}{2} \right) \tilde{G}_\mu^{+a} \left(\frac{z}{2} n \right) | P \rangle \\ &= \left(\bar{U}(P') \gamma_+ \gamma_5 U(P) \tilde{H}^g(x, \xi, t) + \bar{U}(P') \frac{\Delta^+ \gamma_5}{2m_N} U(P) \tilde{E}^g(x, \xi, t) \right), \end{aligned} \quad (\text{C6})$$

$$\tilde{G}^{\mu\nu, a} \equiv \frac{1}{2} \epsilon^{\mu\nu\alpha\beta} G_{\alpha\beta}^a, \quad \mathcal{L} \left(-\frac{z}{2}, \frac{z}{2} \right) \equiv \mathcal{P} \exp \left(i \int_{-z/2}^{z/2} d\zeta A^+(\zeta) \right), \quad (\text{C7})$$

where \mathcal{L} is the standard path-ordered gauge link. The skewedness variable ξ was defined in (30); for quarkonia pair production, it might be expressed as a function of y_1 , y_2 , Q^2 . In the light-cone gauge $A^+ = 0$, we may rewrite the two-gluon operators in (C5) and (C6) as

$$G^{+\mu_\perp a}(z_1) G_{\mu_\perp}^{+a}(z_2) = g_{\mu\nu}^\perp (\partial^+ A^{\mu_\perp a}(z_1)) (\partial^+ A^{\nu_\perp a}(z_2)), \quad (\text{C8})$$

$$\begin{aligned} G^{+\mu_\perp a}(z_1) \tilde{G}_{\mu_\perp}^{+a}(z_2) &= G^{+\mu_\perp a}(z_1) \tilde{G}_{-\mu_\perp}^a(z_2) \\ &= \frac{1}{2} \epsilon_{-\mu_\perp \alpha \nu} G^{+\mu_\perp a}(z_1) G^{\alpha \nu, a}(z_2) \\ &= \epsilon_{-\mu_\perp + \nu_\perp} G^{+\mu_\perp a}(z_1) G^{+\nu_\perp, a}(z_2) \\ &= \epsilon_{\mu\nu}^\perp G^{+\mu_\perp a}(z_1) G^{+\nu_\perp, a}(z_2) \\ &= \epsilon_{\mu\nu}^\perp (\partial^+ A^{\mu, a}(z_1)) (\partial^+ A^{\nu, a}(z_2)). \end{aligned} \quad (\text{C9})$$

After taking the integral over z in (C5) and (C6), we effectively switch to the momentum space, where the derivatives $\partial_{z_1}^+$, $\partial_{z_2}^+$ will turn into the factors $k_{1,2}^+ \sim (x \pm \xi) \bar{P}^+$, so we may rewrite (C5) and (C6) as [40]

$$\begin{aligned} &\frac{1}{\bar{P}^+} \int \frac{dz}{2\pi} e^{ix\bar{P}^+} \left\langle P' \left| A_\mu^a \left(-\frac{z}{2} n \right) A_\nu^b \left(\frac{z}{2} n \right) \right| P \right\rangle \Big|_{A^+=0 \text{ gauge}} \\ &= \frac{\delta^{ab}}{N_c^2 - 1} \left(\frac{-g_{\mu\nu}^\perp F^g(x, \xi, t) - \epsilon_{\mu\nu}^\perp \tilde{F}^g(x, \xi, t)}{2(x - \xi + i0)(x + \xi - i0)} \right). \end{aligned} \quad (\text{C10})$$

We may see that it is possible to extract the coefficient functions C_a and \tilde{C}_a , convoluting Lorentz indices of t -channel gluons in diagrams of Figs. 3 and 4 with $g_{\mu\nu}^\perp$ and $\epsilon_{\mu\nu}^\perp$, respectively, and following [40] we assume that the variable ξ in the denominator is always replaced as $\xi \rightarrow \xi - i0$ in order to define proper contour deformation near the poles of the amplitude.

For evaluation of the coefficient functions, we also need to make proper projections of the $\bar{Q}Q$ pairs onto the states with definite color and spins. According to potential models and NRQCD, the dominant Fock state in quarkonium is the color singlet $\bar{Q}Q$ pair in the ${}^3S_1^{[1]}$ state for J/ψ and the ${}^1S_0^{[1]}$ state for η_c . As discussed in [33,34,40], the projectors on color singlet and color octet states are given, respectively, by

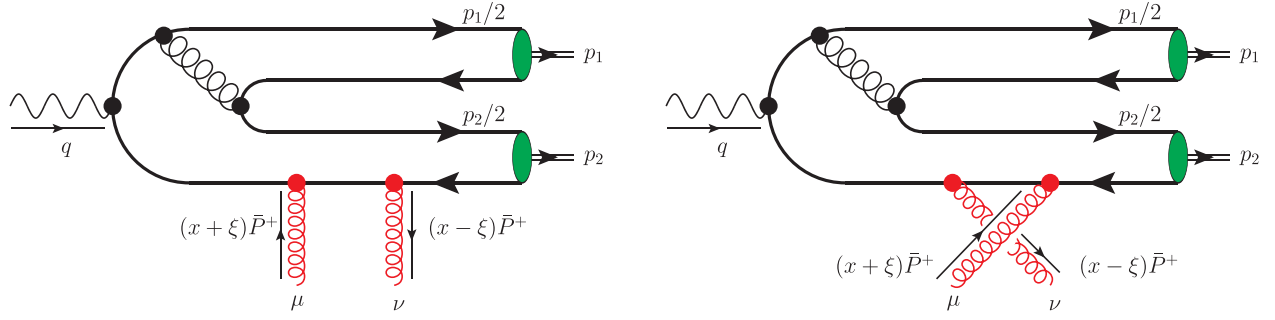


FIG. 12. Schematic illustration of the diagrams with direct and permuted t -channel gluons, which are related to each other by inversion of sign in front of light-cone fraction $x \leftrightarrow -x$ and permutation of the Lorentz indices $\mu \leftrightarrow \nu$.

$$(P^{[1]})_{ij} = \frac{\delta_{ij}}{\sqrt{N_c}}, \quad (P_b^{[8]})_{ij} = \sqrt{2}(t^b)_{ij}, \quad b = 1, \dots, 8. \quad (\text{C11})$$

The projections onto a state with definite total spin S and its projection S_z in the NRQCD picture might be found using proper Clebsch-Gordan coefficients [33,34,40],

$$\hat{P}_{SS_z} = \sum_{s_1, s_2} \left\langle \frac{1}{2} s_1 \frac{1}{2} s_2 | SS_z \right\rangle v \left(\frac{p}{2} - q, s_2 \right) \bar{u} \left(\frac{p}{2} + q, s_1 \right) = \begin{cases} \frac{-1}{2\sqrt{2}} \left(\frac{\hat{p}}{2} - \hat{q} - m_Q \right) \gamma_5 \left(\frac{\hat{p}}{2} + \hat{q} + m_Q \right), & S = 0, \\ \frac{-1}{2\sqrt{2}} \left(\frac{\hat{p}}{2} - \hat{q} - m_Q \right) \hat{\epsilon}_{J/\psi}^*(P) \left(\frac{\hat{p}}{2} + \hat{q} + m_Q \right), & S = 1, \end{cases} \quad (\text{C12})$$

where p is the momentum of the produced quarkonium, $q \approx 0$ is the momentum of relative motion of the quarks inside the quarkonium, and $\epsilon_{J/\psi}$ is the polarization vector of J/ψ mesons. Combining these projectors with proper

color singlet LDMEs and disregarding momentum of the relative motion q , after some algebra we may obtain effective projectors of heavy quarks onto J/ψ and η_c states,

$$(\hat{V}_{\eta_c}^{[1]})_{ij} = -\sqrt{\frac{\langle \mathcal{O}_{\eta_c}^{[1]} \rangle}{m_Q}} \frac{\delta_{ij}}{8N_c m_Q} \left(\frac{\hat{p}}{2} - \hat{q} - m_Q \right) \gamma_5 \left(\frac{\hat{p}}{2} + \hat{q} + m_Q \right) \approx -\sqrt{\frac{\langle \mathcal{O}_{\eta_c}^{[1]} \rangle}{m_Q}} \frac{\delta_{ij}}{4N_c} \left(\frac{\hat{p}}{2} - m_Q \right) \gamma_5, \quad (\text{C13})$$

$$(\hat{V}_{J/\psi}^{[1]})_{ij} = -\sqrt{\frac{\langle \mathcal{O}_{J/\psi}^{[1]} \rangle}{m_Q}} \frac{\delta_{ij}}{8N_c m_Q} \left(\frac{\hat{p}}{2} - \hat{q} - m_Q \right) \hat{\epsilon}_{J/\psi}^*(p) \left(\frac{\hat{p}}{2} + \hat{q} + m_Q \right) \approx \sqrt{\frac{\langle \mathcal{O}_{J/\psi}^{[1]} \rangle}{m_Q}} \frac{\delta_{ij}}{4N_c} \hat{\epsilon}_{J/\psi}^*(p) \left(\frac{\hat{p}}{2} + m_Q \right), \quad (\text{C14})$$

where $\langle \mathcal{O}_M^{[1]} \rangle$ are the corresponding color singlet long-distance matrix elements for J/ψ and η_c mesons. These objects can be related to the radial wave functions in potential model, and for the S -wave quarkonia [32,40] this relation has a form

$$\langle \mathcal{O}_M^{[1]} \rangle = \frac{N_c}{2\pi} |R_S(0)|^2. \quad (\text{C15})$$

Phenomenological estimates, for example, based on analysis of the partial decay width of $J/\psi \rightarrow e^+ e^-$, suggest that $\langle \mathcal{O}_{J/\psi}^{[1]}(^3S_1^{[1]}) \rangle \approx \langle \mathcal{O}_{\eta_c}^{[1]}(^1S_0^{[1]}) \rangle \approx 0.3 \text{ GeV}^3$ [86].

In evaluation of the diagrams from Figs. 3 and 4, we should take into account that each diagram should be

accompanied with another diagram with permuted final-state mesons $1 \leftrightarrow 2$ (equivalently, a diagram with inverted direction of quark lines), as well as a diagram with permutation of t -channel gluons, as shown in Fig. 12. The latter permutation gives contributions that differ only by change of the sign in front of the light-cone variable x and interchange of the Lorentz indices $\mu \leftrightarrow \nu$. According to (C10), we need to contract the free Lorentz indices μ, ν with symmetric $g_{\mu\nu}^\perp$ or antisymmetric $\epsilon_{\mu\nu}^\perp$ in order to single out the contributions of F^g or \tilde{F}^g ; for this reason, eventually, we conclude that the coefficient functions C_a, \tilde{C}_a will be even or odd functions of the variable x , respectively. Since we disregard internal motion of quarks inside quarkonia, the momenta of all partons are fixed by energy-momentum

conservation and could be expressed as linear combinations of the momenta of the quarkonia and t -channel gluons. Taking into account (C10), (C13), and (C14), we may obtain for the coefficient functions

$$C_a(x, \tilde{y}_1, \tilde{y}_2) = \kappa \frac{C_a(x, \tilde{y}_1, \tilde{y}_2) + C_a(-x, \tilde{y}_1, \tilde{y}_2)}{(x - \xi + i0)(x + \xi - i0)}, \quad (\text{C16})$$

$$\tilde{C}_a(x, \tilde{y}_1, \tilde{y}_2) = \kappa \frac{\tilde{C}_a(x, \tilde{y}_1, \tilde{y}_2) - \tilde{C}_a(-x, \tilde{y}_1, \tilde{y}_2)}{(x - \xi + i0)(x + \xi - i0)}, \quad (\text{C17})$$

where the constant κ is defined as

$$\kappa = (4\pi\alpha_s)^2 e_Q \frac{\sqrt{\langle \mathcal{O}_{J/\psi}^{[1]}(3S_1^{[1]}) \rangle \langle \mathcal{O}_{\eta_c}^{[1]}(1S_0^{[1]}) \rangle}}{4N_c^2 m_Q} (\epsilon_{J/\psi}^* \cdot \epsilon_T^{(\gamma)}), \quad (\text{C18})$$

and the factors $x \pm \xi \mp i0$ in denominators of (C16) and (C17) stem from (C10). The contribution of each diagram from Figs. 3 and 4 to functions C_a and \tilde{C}_a might be obtained taking Dirac and color traces over the heavy quark loop and contracting free Lorentz indices μ, ν with $g_{\mu\nu}^\perp$ or $\epsilon_{\mu\nu}^\perp$, respectively; this operation was done using the FeynCalc package for *Mathematica* [99,100]. We need to mention that gluon GPDs H^g, E^g are even functions of variable x , whereas \tilde{H}^g, \tilde{E}^g are odd functions [3]; for this reason, in

convolution over x both terms in the numerators of (C16) and (C17) give equal nonzero contributions. Numerically, the dominant contribution comes from GPD H^g , whereas contribution of \tilde{H}^g is negligibly small. As we will see below, the functions C_a, \tilde{C}_a might have other poles as a function of x , so the structure of the functions C_a, \tilde{C}_a might be represented schematically as a sum (37).

The explicit expressions for the functions C_a, \tilde{C}_a depend on polarizations of the photon and are given by

$$C_L = \mathcal{O}(p_{a\perp}/Q, p_{a\perp}/m_Q) \approx 0, \quad (\text{C19})$$

$$C_T = \frac{N_c^2 - 1}{4N_c} \sum_{k=1}^7 a_k - \frac{1}{4N_c} \sum_{k=1}^3 b_k + \frac{N_c}{4} \sum_{k=1}^5 c_k + \frac{1}{4} \sum_{k=1}^2 d_k, \quad (\text{C20})$$

$$\tilde{C}_T = \frac{N_c^2 - 1}{4N_c} \sum_{k=1}^7 \tilde{a}_k - \frac{1}{4N_c} \sum_{k=1}^3 \tilde{b}_k + \frac{N_c}{4} \sum_{k=1}^5 \tilde{c}_k + \frac{1}{4} \sum_{k=1}^2 \tilde{d}_k, \quad (\text{C21})$$

where the contributions $a_i, b_i, \tilde{a}_i, \tilde{b}_i$ stem from the diagrams without three-gluon vertices in Fig. 3, the terms c_i, \tilde{c}_i come from the diagrams that include at least one three-gluon vertex, and the terms d_i, \tilde{d}_i stem from the diagrams in Fig. 4. Explicitly, these contributions are given by

$$a_1 = 4e^{\tilde{y}_1 + \tilde{y}_2} Z(e^{\tilde{y}_1 + \tilde{y}_2} Q^2 + 4(e^{\tilde{y}_1} + e^{\tilde{y}_2}) m_Q^2 Z)(x + \xi) \left[m_Q(4e^{\tilde{y}_1} m_Q^2 (e^{\tilde{y}_1} - Z)Z + (e^{2\tilde{y}_2} + 2e^{\tilde{y}_2}(e^{\tilde{y}_1} - Z))(e^{\tilde{y}_1} Q^2 + 4m_Q^2 Z)) \right. \\ \left. \times ((e^{\tilde{y}_1} Q^2 + 4m_Q^2 Z)(e^{2\tilde{y}_2} + 2e^{\tilde{y}_2}(e^{\tilde{y}_1} - x - Z - \xi)) + 4e^{\tilde{y}_1} m_Q^2 Z(e^{\tilde{y}_1} - x - Z - \xi))(1 + \cosh(\tilde{y}_1 - \tilde{y}_2)) \right]^{-1}, \quad (\text{C22})$$

$$a_2 = \frac{2e^{2\tilde{y}_2}(e^{\tilde{y}_1} + e^{\tilde{y}_2})Z(e^{\tilde{y}_1 + \tilde{y}_2} Q^2 + 4m_Q^2 Z^2)}{m_Q(e^{\tilde{y}_1} + e^{\tilde{y}_2} - 2Z)(e^{\tilde{y}_1 + \tilde{y}_2} Q^2 + 2(e^{\tilde{y}_1} + e^{\tilde{y}_2}) m_Q^2 Z)(-e^{2\tilde{y}_2} Q^2 + e^{\tilde{y}_2} Q^2 Z + 4m_Q^2 Z^2)\xi}, \quad (\text{C23})$$

$$a_3 = 8e^{\tilde{y}_1 + \tilde{y}_2} Z(e^{\tilde{y}_1 + 2\tilde{y}_2} Q^2 - 8e^{\tilde{y}_1} m_Q^2 Z^2 - 2e^{\tilde{y}_2} Z(e^{\tilde{y}_1} Q^2 + 2m_Q^2 Z)) \left[(e^{\tilde{y}_1} + e^{\tilde{y}_2}) m_Q (e^{2\tilde{y}_2} Q^2 - e^{\tilde{y}_2} Q^2 Z - 4m_Q^2 Z^2) \right. \\ \left. \times ((2e^{\tilde{y}_2} + e^{\tilde{y}_1} - 2Z)e^{\tilde{y}_1 + \tilde{y}_2} Q^2 + 4m_Q^2 Z(e^{\tilde{y}_1}(e^{\tilde{y}_1} - 2Z) + e^{2\tilde{y}_2} - e^{\tilde{y}_2}(Z - 2e^{\tilde{y}_1}))) \right]^{-1}, \quad (\text{C24})$$

$$a_4 = -8e^{\tilde{y}_1 + 2\tilde{y}_2} Z(e^{\tilde{y}_1 + \tilde{y}_2} Q^2 + 4m_Q^2 Z^2) \left[m_Q(e^{\tilde{y}_1} + e^{\tilde{y}_2} - 2Z)(e^{2\tilde{y}_2} Q^2 - 2e^{\tilde{y}_2} Q^2 Z - 4m_Q^2 Z^2) \right. \\ \left. \times ((2e^{\tilde{y}_2} + e^{\tilde{y}_1} - 2Z)e^{\tilde{y}_1 + \tilde{y}_2} Q^2 + 4m_Q^2 Z(e^{\tilde{y}_1}(e^{\tilde{y}_1} - 2Z) + e^{2\tilde{y}_2} - e^{\tilde{y}_2}(Z - 2e^{\tilde{y}_1}))) \right]^{-1}, \quad (\text{C25})$$

$$a_5 = 8e^{2(\tilde{y}_1 + \tilde{y}_2)} Q^2 Z(e^{\tilde{y}_1 + \tilde{y}_2} Q^2 + 4m_Q^2 Z(-x + Z + \xi)) \left[m_Q(e^{\tilde{y}_1 + \tilde{y}_2} Q^2 + 2(e^{\tilde{y}_1} + e^{\tilde{y}_2}) m_Q^2 Z)(-e^{2\tilde{y}_2} Q^2 + 2e^{\tilde{y}_2} Q^2 Z + 4m_Q^2 Z^2) \right. \\ \left. \times (e^{\tilde{y}_1} + e^{\tilde{y}_2} + 2x - 2Z - 2\xi)(-e^{2\tilde{y}_1} Q^2 - 2e^{\tilde{y}_1} Q^2(x - Z - \xi) + 4m_Q^2 Z(-x + Z + \xi)) \right]^{-1}, \quad (\text{C26})$$

$$a_6 = 16e^{\tilde{y}_1+2\tilde{y}_2}m_Q Z^2(Q^2 e^{\tilde{y}_2}(e^{2\tilde{y}_2} - 2e^{\tilde{y}_1}Z + e^{\tilde{y}_2}(e^{\tilde{y}_1} - 2(x+Z+\xi))) - 4m_Q^2 Z^2(e^{\tilde{y}_1} + e^{\tilde{y}_2})) \\ \times \left[(e^{\tilde{y}_1+\tilde{y}_2}Q^2 + 2(e^{\tilde{y}_1} + e^{\tilde{y}_2})m_Q^2 Z)(e^{2\tilde{y}_2}Q^2 - 2e^{\tilde{y}_2}Q^2 Z - 4m_Q^2 Z^2)(e^{\tilde{y}_1} + e^{\tilde{y}_2} - 2(x+Z+\xi)) \right. \\ \left. \times (e^{2\tilde{y}_2}(e^{\tilde{y}_1}Q^2 + 4m_Q^2 Z) + 4e^{\tilde{y}_1}m_Q^2 Z(e^{\tilde{y}_1} - x - Z - \xi) + 2e^{\tilde{y}_2}(e^{\tilde{y}_1}Q^2 + 4m_Q^2 Z)(e^{\tilde{y}_1} - x - Z - \xi)) \right]^{-1}, \quad (C27)$$

$$a_7 = \frac{4e^{2\tilde{y}_2}Q^2 Z(x+\xi)}{m_Q(2e^{\tilde{y}_2}Q^2 Z - e^{2\tilde{y}_2}Q^2 + 4m_Q^2 Z^2)(2e^{\tilde{y}_2}Q^2(x+Z+\xi) - e^{2\tilde{y}_2}Q^2 + 4m_Q^2 Z(x+Z+\xi))(1 + \cosh(\tilde{y}_1 - \tilde{y}_2))}, \quad (C28)$$

$$b_1 = \frac{-8e^{3\tilde{y}_1+\tilde{y}_2}Q^2 Z}{m_Q(e^{\tilde{y}_1+\tilde{y}_2}Q^2 + 2(e^{\tilde{y}_1} + e^{\tilde{y}_2})m_Q^2 Z)(e^{2\tilde{y}_1}Q^2 - 2e^{\tilde{y}_1}Q^2 Z - 4m_Q^2 Z^2)(e^{\tilde{y}_1} + e^{\tilde{y}_2} + 2x - 2Z - 2\xi)}, \quad (C29)$$

$$b_2 = -\frac{4e^{\tilde{y}_1+\tilde{y}_2}(e^{\tilde{y}_1}Q^2 + 2m_Q^2 Z)}{(e^{\tilde{y}_1} + e^{\tilde{y}_2})m_Q^3(e^{2\tilde{y}_1}Q^2 - 2e^{\tilde{y}_1}Q^2(x+Z+\xi) - 4m_Q^2 Z(x+Z+\xi))}, \quad (C30)$$

$$b_3 = \frac{1}{(e^{\tilde{y}_1} + e^{\tilde{y}_2})m_Q} \frac{8e^{\tilde{y}_1+\tilde{y}_2}Z(-e^{3\tilde{y}_1}Q^2 - e^{2\tilde{y}_1+\tilde{y}_2}Q^2 + 2e^{\tilde{y}_1+\tilde{y}_2}Q^2 Z + 2e^{2\tilde{y}_1}Q^2(x+Z+\xi) + 4m_Q^2 Z^2(e^{\tilde{y}_1} + e^{\tilde{y}_2}))}{(Q^2(e^{2\tilde{y}_1} - 2e^{\tilde{y}_1}Z) - 4m_Q^2 Z^2)(e^{\tilde{y}_1} + e^{\tilde{y}_2} + 2x - 2\xi)(Q^2(e^{2\tilde{y}_1} - 2e^{\tilde{y}_1}(x+Z+\xi)) - 4m_Q^2 Z(x+Z+\xi))}, \quad (C31)$$

$$c_1 = 2e^{2\tilde{y}_1+\tilde{y}_2} \left[e^{4\tilde{y}_2}(-3x+\xi) - 2e^{3\tilde{y}_2}(e^{\tilde{y}_1}(6x-2\xi) + \xi(-5x+\xi)) + e^{2\tilde{y}_1}(e^{\tilde{y}_1} - 4\xi)(2(x-\xi)\xi + e^{\tilde{y}_1}(-3x+\xi)) \right. \\ \left. - 2e^{\tilde{y}_1+\tilde{y}_2}(e^{2\tilde{y}_1}(6x-2\xi) + e^{\tilde{y}_1}\xi(-19x+7\xi) + 2\xi(-2x^2+5x\xi+\xi^2)) - 2e^{2\tilde{y}_2}(e^{2\tilde{y}_1}(9x-3\xi) \right. \\ \left. + e^{\tilde{y}_1}\xi(-17x+5\xi) + 4\xi(x^2+x\xi-\xi^2)) \right] \left[(e^{\tilde{y}_1} + e^{\tilde{y}_2})^2 m_Q^3 (e^{2\tilde{y}_2} + e^{\tilde{y}_1}(e^{\tilde{y}_1} - 2\xi) + 2e^{\tilde{y}_2}(e^{\tilde{y}_1} - 2\xi)) \right. \\ \left. \times (e^{2\tilde{y}_2} + e^{\tilde{y}_1}(e^{\tilde{y}_1} - 4\xi) + 2e^{\tilde{y}_2}(e^{\tilde{y}_1} - \xi))(x-\xi)(e^{\tilde{y}_1} + e^{\tilde{y}_2} - 2(x+\xi)) \right]^{-1}, \quad (C32)$$

$$c_2 = -2e^{\tilde{y}_1+\tilde{y}_2} \left[e^{5\tilde{y}_1}(x-3\xi) + e^{3\tilde{y}_2}(e^{\tilde{y}_2} - 4\xi)(e^{\tilde{y}_2} - 2\xi)(-x+\xi) + 2e^{3\tilde{y}_1}(e^{2\tilde{y}_2}(x-7\xi) - 2e^{\tilde{y}_2}(5x-11\xi)\xi + 12(x-\xi)\xi^2) \right. \\ \left. + e^{4\tilde{y}_1}(e^{\tilde{y}_2}(3x-11\xi) + 2\xi(-5x+9\xi)) + e^{\tilde{y}_1+2\tilde{y}_2}(4e^{\tilde{y}_2}(3x-\xi)\xi + e^{2\tilde{y}_2}(-3x+\xi) - 4\xi(-2x^2+3x\xi+\xi^2)) \right. \\ \left. - 2e^{2\tilde{y}_1+\tilde{y}_2}(2e^{\tilde{y}_2}(x-7\xi)\xi + e^{2\tilde{y}_2}(x+3\xi) + 2\xi(2x^2-5x\xi+7\xi^2)) \right] \left[(e^{\tilde{y}_1} + e^{\tilde{y}_2})m_Q^3 (e^{2\tilde{y}_2} + e^{\tilde{y}_1}(e^{\tilde{y}_1} - 2\xi) \right. \\ \left. + 2e^{\tilde{y}_2}(e^{\tilde{y}_1} - 2\xi))(e^{\tilde{y}_1} + e^{\tilde{y}_2} - 4\xi)(e^{2\tilde{y}_2} + e^{\tilde{y}_1}(e^{\tilde{y}_1} - 4\xi) + 2e^{\tilde{y}_2}(e^{\tilde{y}_1} - \xi))(e^{\tilde{y}_1} + e^{\tilde{y}_2} + 2x - 2\xi)(x-\xi) \right]^{-1}, \quad (C33)$$

$$c_3 = \frac{2e^{2\tilde{y}_1+\tilde{y}_2}(2e^{2\tilde{y}_1} + 2e^{2\tilde{y}_2} + 4e^{\tilde{y}_1+\tilde{y}_2} - 2e^{\tilde{y}_1}(x+\xi) - e^{\tilde{y}_2}(x+\xi))}{(e^{\tilde{y}_1} + e^{\tilde{y}_2})^2 m_Q^3 (e^{\tilde{y}_1} + e^{\tilde{y}_2} - 2(x+\xi))(e^{2\tilde{y}_1} + e^{2\tilde{y}_2} + 2e^{\tilde{y}_1+\tilde{y}_2} - 2e^{\tilde{y}_1}(x+\xi) - e^{\tilde{y}_2}(x+\xi))}, \quad (C34)$$

$$c_4 = -\frac{2e^{2(\tilde{y}_1+\tilde{y}_2)}}{(e^{\tilde{y}_1} + e^{\tilde{y}_2})^2 m_Q^3 (e^{\tilde{y}_1} + e^{\tilde{y}_2} - 2(x+\xi))} \\ \times \left[\frac{4e^{2\tilde{y}_1}\xi + 4e^{2\tilde{y}_2}\xi + 8e^{\tilde{y}_1+\tilde{y}_2}\xi - 4e^{\tilde{y}_1}\xi(x+\xi) - 2e^{\tilde{y}_2}(x+\xi)(x+3\xi)}{(e^{2\tilde{y}_2} + e^{\tilde{y}_1}(e^{\tilde{y}_1} - 2\xi) + 2e^{\tilde{y}_2}(e^{\tilde{y}_1} - 2\xi))(e^{2\tilde{y}_1} + e^{2\tilde{y}_2} + 2e^{\tilde{y}_1+\tilde{y}_2} - e^{\tilde{y}_1}(x+\xi) - 2e^{\tilde{y}_2}(x+\xi))} \right. \\ \left. - \frac{(x+\xi)(e^{2\tilde{y}_2} + 2e^{\tilde{y}_2}(e^{\tilde{y}_1} - \xi) + e^{\tilde{y}_1}(e^{\tilde{y}_1} - 2(x+\xi)))}{(e^{2\tilde{y}_2} + e^{\tilde{y}_1}(e^{\tilde{y}_1} - 4\xi) + 2e^{\tilde{y}_2}(e^{\tilde{y}_1} - \xi))(e^{2\tilde{y}_1} + e^{2\tilde{y}_2} + 2e^{\tilde{y}_1+\tilde{y}_2} - 2e^{\tilde{y}_1}(x+\xi) - e^{\tilde{y}_2}(x+\xi))} \right], \quad (C35)$$

$$c_5 = \frac{2e^{\tilde{y}_1+2\tilde{y}_2}(5(e^{\tilde{y}_1} + e^{\tilde{y}_2}) + 4(x+4\xi))}{(e^{\tilde{y}_1} + e^{\tilde{y}_2})^2 m_Q^3 (e^{\tilde{y}_1} + e^{\tilde{y}_2} + 4\xi)(e^{\tilde{y}_1} + e^{\tilde{y}_2} + 2x + 6\xi)}, \quad (C36)$$

$$d_1 = -4e^{\bar{y}_1+\bar{y}_2}Z(e^{\bar{y}_1+2\bar{y}_2}Q^2 - 4e^{\bar{y}_1}m_Q^2Z^2 + e^{\bar{y}_2}(-e^{2\bar{y}_1}Q^2 + 4m_Q^2Z^2 + e^{\bar{y}_1}Q^2(x - 2Z + \xi))) \\ \times \left[m_Q(2e^{\bar{y}_2}Q^2Z - e^{2\bar{y}_2}Q^2 + 4m_Q^2Z^2)(e^{\bar{y}_1} - x - \xi)(e^{2\bar{y}_2}(e^{\bar{y}_1}Q^2 - 4m_Q^2Z) \right. \\ \left. - 4e^{\bar{y}_1}m_Q^2Z(e^{\bar{y}_1} - x + Z - \xi) - 2e^{\bar{y}_2}(e^{\bar{y}_1}Q^2 - 4m_Q^2Z)(e^{\bar{y}_1} - x + Z - \xi)) \right]^{-1}, \quad (C37)$$

$$d_2 = -\frac{8e^{\bar{y}_1+\bar{y}_2}Z(e^{2\bar{y}_2}Q^2 - 4m_Q^2Z^2 - e^{\bar{y}_2}Q^2(x + 2Z + \xi))}{m_Q(2e^{\bar{y}_2}Q^2Z - e^{2\bar{y}_2}Q^2 + 4m_Q^2Z^2)(e^{\bar{y}_1} - x - \xi)(2e^{\bar{y}_2}Q^2(x + Z + \xi) - e^{2\bar{y}_2}Q^2 + 4m_Q^2Z(x + Z + \xi))}, \quad (C38)$$

$$\tilde{a}_1 = 8e^{2(\bar{y}_1+\bar{y}_2)}Z(e^{\bar{y}_1+\bar{y}_2}Q^2 + 4e^{\bar{y}_1}m_Q^2Z + 4e^{\bar{y}_2}m_Q^2Z)(x + \xi) \left[(e^{\bar{y}_1} + e^{\bar{y}_2})^2m_Q(e^{2\bar{y}_2}(e^{\bar{y}_1}Q^2 + 4m_Q^2Z) \right. \\ \left. + 4e^{\bar{y}_1}m_Q^2Z(e^{\bar{y}_1} - x - Z - \xi) + 2e^{\bar{y}_2}(e^{\bar{y}_1}Q^2 + 4m_Q^2Z)(e^{\bar{y}_1} - x - Z - \xi)) \right. \\ \left. \times (e^{2\bar{y}_2}(e^{\bar{y}_1}Q^2 + 4m_Q^2Z) + 2e^{\bar{y}_2}(e^{\bar{y}_1} - Z)(e^{\bar{y}_1}Q^2 + 4m_Q^2Z) + 4e^{\bar{y}_1}m_Q^2(e^{\bar{y}_1} - Z)Z) \right]^{-1}, \quad (C39)$$

$$\tilde{a}_2 = \frac{2e^{2\bar{y}_2}(e^{\bar{y}_1} + e^{\bar{y}_2})Z(e^{\bar{y}_1+\bar{y}_2}Q^2 + 4m_Q^2Z^2)}{m_Q(e^{\bar{y}_1} + e^{\bar{y}_2} - 2Z)(e^{\bar{y}_1+\bar{y}_2}Q^2 + 2m_Q^2Z(e^{\bar{y}_1} + e^{\bar{y}_2}))}(e^{2\bar{y}_2}Q^2 - 2e^{\bar{y}_2}Q^2Z - 4m_Q^2Z^2)\xi, \quad (C40)$$

$$\tilde{a}_3 = 8e^{\bar{y}_1+\bar{y}_2}Z(e^{\bar{y}_1+2\bar{y}_2}Q^2 - 8e^{\bar{y}_1}m_Q^2Z^2 - 2e^{\bar{y}_2}Z(e^{\bar{y}_1}Q^2 + 2m_Q^2Z)) \left[(e^{\bar{y}_1} + e^{\bar{y}_2})m_Q(e^{2\bar{y}_2}Q^2 - 2e^{\bar{y}_2}Q^2Z - 4m_Q^2Z^2) \right. \\ \left. \times (4e^{\bar{y}_1}m_Q^2(e^{\bar{y}_1} - 2Z)Z + 2e^{2\bar{y}_2}(e^{\bar{y}_1}Q^2 + 2m_Q^2Z) + e^{\bar{y}_2}(e^{2\bar{y}_1}Q^2 - 2e^{\bar{y}_1}(-4m_Q^2 + Q^2)Z - 4m_Q^2Z^2)) \right]^{-1}, \quad (C41)$$

$$\tilde{a}_4 = 8e^{\bar{y}_1+2\bar{y}_2}Z(e^{\bar{y}_1+\bar{y}_2}Q^2 + 4m_Q^2Z^2) \left[m_Q(e^{\bar{y}_1} + e^{\bar{y}_2} - 2Z)(e^{2\bar{y}_2}Q^2 - 2e^{\bar{y}_2}Q^2Z - 4m_Q^2Z^2) \right. \\ \left. \times (4e^{\bar{y}_1}m_Q^2(e^{\bar{y}_1} - 2Z)Z + 2e^{2\bar{y}_2}(e^{\bar{y}_1}Q^2 + 2m_Q^2Z) + e^{\bar{y}_2}(e^{2\bar{y}_1}Q^2 - 2e^{\bar{y}_1}(-4m_Q^2 + Q^2)Z - 4m_Q^2Z^2)) \right]^{-1}, \quad (C42)$$

$$\tilde{a}_5 = 8e^{2(\bar{y}_1+\bar{y}_2)}Q^2Z(e^{\bar{y}_1+\bar{y}_2}Q^2 + 4m_Q^2Z(-x + Z + \xi)) \left[m_Q(e^{\bar{y}_1+\bar{y}_2}Q^2 + 2m_Q^2Z(e^{\bar{y}_1} + e^{\bar{y}_2}))(-e^{2\bar{y}_2}Q^2 + 2e^{\bar{y}_2}Q^2Z + 4m_Q^2Z^2) \right. \\ \left. \times (e^{\bar{y}_1} + e^{\bar{y}_2} + 2x - 2Z - 2\xi)(-e^{2\bar{y}_1}Q^2 - 2e^{\bar{y}_1}Q^2(x - Z - \xi) + 4m_Q^2Z(-x + Z + \xi)) \right]^{-1}, \quad (C43)$$

$$\tilde{a}_6 = -16e^{\bar{y}_1+2\bar{y}_2}m_QZ^2(e^{3\bar{y}_2}Q^2 - 4e^{\bar{y}_1}m_Q^2Z^2 - 2e^{\bar{y}_2}Z(e^{\bar{y}_1}Q^2 + 2m_Q^2Z) + e^{2\bar{y}_2}Q^2(e^{\bar{y}_1} - 2(x + Z + \xi))) \\ \times \left[(e^{\bar{y}_1+\bar{y}_2}Q^2 + 2m_Q^2Z(e^{\bar{y}_1} + e^{\bar{y}_2}))(-e^{2\bar{y}_2}Q^2 - 2e^{\bar{y}_2}Q^2Z - 4m_Q^2Z^2)(e^{2\bar{y}_2}(e^{\bar{y}_1}Q^2 + 4m_Q^2Z) \right. \\ \left. + 4e^{\bar{y}_1}m_Q^2Z(e^{\bar{y}_1} - x - Z - \xi) + 2e^{\bar{y}_2}(e^{\bar{y}_1}Q^2 + 4m_Q^2Z)(e^{\bar{y}_1} - x - Z - \xi)) \right. \\ \left. \times (e^{\bar{y}_1} + e^{\bar{y}_2} - 2(x + Z + \xi)) \right]^{-1}, \quad (C44)$$

$$\tilde{a}_7 = -\frac{8e^{\bar{y}_1+3\bar{y}_2}Q^2Z(x + \xi)}{(e^{\bar{y}_1} + e^{\bar{y}_2})^2m_Q(e^{2\bar{y}_2}Q^2 - 2e^{\bar{y}_2}Q^2Z - 4m_Q^2Z^2)(e^{2\bar{y}_2}Q^2 - 2e^{\bar{y}_2}Q^2(x + Z + \xi) - 4m_Q^2Z(x + Z + \xi))}, \quad (C45)$$

$$\tilde{b}_1 = \frac{8e^{3\bar{y}_1+\bar{y}_2}Q^2Z}{m_Q(e^{\bar{y}_1+\bar{y}_2}Q^2 + 2m_Q^2Z(e^{\bar{y}_1} + e^{\bar{y}_2}))}(e^{2\bar{y}_1}Q^2 - 2e^{\bar{y}_1}Q^2Z - 4m_Q^2Z^2)(e^{\bar{y}_1} + e^{\bar{y}_2} + 2x - 2Z - 2\xi), \quad (C46)$$

$$\tilde{b}_2 = \frac{4e^{\bar{y}_1+\bar{y}_2}(e^{\bar{y}_1}Q^2 + 2m_Q^2Z)}{(e^{\bar{y}_1} + e^{\bar{y}_2})m_Q^3(e^{2\bar{y}_1}Q^2 - 2e^{\bar{y}_1}Q^2(x + Z + \xi) - 4m_Q^2Z(x + Z + \xi))}, \quad (C47)$$

$$\tilde{b}_3 = \frac{8e^{\bar{y}_1+\bar{y}_2}Z(e^{3\bar{y}_1}Q^2 + e^{2\bar{y}_1+\bar{y}_2}Q^2 - 2e^{\bar{y}_1+\bar{y}_2}Q^2Z - 4(e^{\bar{y}_1} + e^{\bar{y}_2})m_Q^2Z^2 - 2e^{2\bar{y}_1}Q^2(x + Z + \xi))(e^{\bar{y}_1} + e^{\bar{y}_2})^{-1}}{m_Q(e^{2\bar{y}_1}Q^2 - 2e^{\bar{y}_1}Q^2Z - 4m_Q^2Z^2)(e^{\bar{y}_1} + e^{\bar{y}_2} + 2x - 2\xi)(Q^2(e^{2\bar{y}_1} - 2e^{\bar{y}_1}(x + Z + \xi)) - 4m_Q^2Z(x + Z + \xi))}, \quad (C48)$$

$$\begin{aligned}\tilde{c}_1 = & -2e^{2\bar{y}_1+\bar{y}_2} \left[e^{4\bar{y}_2} + e^{2\bar{y}_1}(e^{\bar{y}_1} - 4\xi)(e^{\bar{y}_1} - 2\xi) + 4e^{3\bar{y}_2}(e^{\bar{y}_1} - \xi) \right. \\ & \left. + 2e^{2\bar{y}_2}(3e^{2\bar{y}_1} - 7e^{\bar{y}_1}\xi - 2\xi(2x + \xi)) + 4e^{\bar{y}_1+\bar{y}_2}(e^{2\bar{y}_1} - 4e^{\bar{y}_1}\xi + \xi(2x + 5\xi)) \right] \\ & \times \left[(e^{\bar{y}_1} + e^{\bar{y}_2})^2 m_Q^3 (e^{2\bar{y}_2} + e^{\bar{y}_1}(e^{\bar{y}_1} - 2\xi) + 2e^{\bar{y}_2}(e^{\bar{y}_1} - 2\xi)) \right. \\ & \left. \times (e^{2\bar{y}_2} + e^{\bar{y}_1}(e^{\bar{y}_1} - 4\xi) + 2e^{\bar{y}_2}(e^{\bar{y}_1} - \xi))(e^{\bar{y}_1} + e^{\bar{y}_2} - 2(x + \xi)) \right]^{-1},\end{aligned}$$

$$\begin{aligned}\tilde{c}_2 = & -2e^{\bar{y}_1+\bar{y}_2} \left[e^{5\bar{y}_1} + e^{4\bar{y}_1}(5e^{\bar{y}_2} - 6\xi) + e^{3\bar{y}_2}(e^{\bar{y}_2} - 4\xi)(e^{\bar{y}_2} - 2\xi) + 2e^{3\bar{y}_1}(5e^{2\bar{y}_2} + e^{\bar{y}_2}(4x - 9\xi) + 4\xi^2) \right. \\ & \left. + e^{\bar{y}_1+2\bar{y}_2}(5e^{2\bar{y}_2} + 2e^{\bar{y}_2}(4x - 9\xi) + 8\xi(-3x + \xi)) + 2e^{2\bar{y}_1+\bar{y}_2}(5e^{2\bar{y}_2} + 4e^{\bar{y}_2}(2x - 3\xi) + 6\xi(-2x + \xi)) \right] \\ & \times \left[(e^{\bar{y}_1} + e^{\bar{y}_2})m_Q^3 (e^{2\bar{y}_2} + e^{\bar{y}_1}(e^{\bar{y}_1} - 2\xi) + 2e^{\bar{y}_2}(e^{\bar{y}_1} - 2\xi))(e^{2\bar{y}_2} + e^{\bar{y}_1}(e^{\bar{y}_1} - 4\xi) \right. \\ & \left. + 2e^{\bar{y}_2}(e^{\bar{y}_1} - \xi))(e^{\bar{y}_1} + e^{\bar{y}_2} - 4\xi)(e^{\bar{y}_1} + e^{\bar{y}_2} + 2x - 2\xi) \right]^{-1},\end{aligned}\quad (C49)$$

$$\begin{aligned}\tilde{c}_3 = & 4e^{\bar{y}_1+\bar{y}_2} \left[e^{5\bar{y}_1} + e^{4\bar{y}_1}(5e^{\bar{y}_2} + x - 5\xi) + e^{\bar{y}_1+2\bar{y}_2}(5e^{\bar{y}_2} + 2(x - 7\xi))(e^{\bar{y}_2} - 2\xi) \right. \\ & \left. + e^{3\bar{y}_2}(e^{\bar{y}_2} + x - 3\xi)(e^{\bar{y}_2} - 2\xi) + 2e^{2\bar{y}_1+\bar{y}_2}(5e^{2\bar{y}_2} + e^{\bar{y}_2}(x - 19\xi) - 2(x - 8\xi)\xi) \right. \\ & \left. + 2e^{3\bar{y}_1}(5e^{2\bar{y}_2} + e^{\bar{y}_2}(x - 12\xi) + \xi(-x + 3\xi)) \right] \left[(e^{\bar{y}_1} + e^{\bar{y}_2})m_Q^3 (e^{2\bar{y}_2} + e^{\bar{y}_1}(e^{\bar{y}_1} - 2\xi) \right. \\ & \left. + 2e^{\bar{y}_2}(e^{\bar{y}_1} - 2\xi))(e^{\bar{y}_1} + e^{\bar{y}_2} - 4\xi)(e^{2\bar{y}_2} + e^{\bar{y}_1}(e^{\bar{y}_1} - 4\xi) + 2e^{\bar{y}_2}(e^{\bar{y}_1} - \xi))(e^{\bar{y}_1} + e^{\bar{y}_2} + 2x - 2\xi) \right]^{-1},\end{aligned}\quad (C50)$$

$$\tilde{c}_4 = \frac{2e^{2\bar{y}_1+\bar{y}_2}(2e^{2\bar{y}_1} + 2e^{2\bar{y}_2} + 4e^{\bar{y}_1+\bar{y}_2} - 2e^{\bar{y}_1}(x + \xi) - e^{\bar{y}_2}(x + \xi))}{(e^{\bar{y}_1} + e^{\bar{y}_2})^2 m_Q^3 (e^{\bar{y}_1} + e^{\bar{y}_2} - 2(x + \xi))(e^{2\bar{y}_1} + e^{2\bar{y}_2} + 2e^{\bar{y}_1+\bar{y}_2} - 2e^{\bar{y}_1}(x + \xi) - e^{\bar{y}_2}(x + \xi))},\quad (C51)$$

$$\begin{aligned}\tilde{c}_5 = & -\frac{2e^{2(\bar{y}_1+\bar{y}_2)}}{(e^{\bar{y}_1} + e^{\bar{y}_2})^2 m_Q^3 (e^{\bar{y}_1} + e^{\bar{y}_2} - 2(x + \xi))} \\ & \times \left(\frac{-4e^{2\bar{y}_1}\xi - 4e^{2\bar{y}_2}\xi - 8e^{\bar{y}_1+\bar{y}_2}\xi + 4e^{\bar{y}_1}\xi(x + \xi) + 2e^{\bar{y}_2}(x + \xi)(x + 3\xi)}{(e^{2\bar{y}_2} + e^{\bar{y}_1}(e^{\bar{y}_1} - 2\xi) + 2e^{\bar{y}_2}(e^{\bar{y}_1} - 2\xi))(e^{2\bar{y}_1} + e^{2\bar{y}_2} + 2e^{\bar{y}_1+\bar{y}_2} - e^{\bar{y}_1}(x + \xi) - 2e^{\bar{y}_2}(x + \xi))} \right. \\ & \left. + \frac{(x + \xi)(e^{2\bar{y}_2} + 2e^{\bar{y}_2}(e^{\bar{y}_1} - \xi) + e^{\bar{y}_1}(e^{\bar{y}_1} - 2(x + \xi)))}{(e^{2\bar{y}_2} + e^{\bar{y}_1}(e^{\bar{y}_1} - 4\xi) + 2e^{\bar{y}_2}(e^{\bar{y}_1} - \xi))(e^{2\bar{y}_1} + e^{2\bar{y}_2} + 2e^{\bar{y}_1+\bar{y}_2} - 2e^{\bar{y}_1}(x + \xi) - e^{\bar{y}_2}(x + \xi))} \right),\end{aligned}\quad (C52)$$

$$\tilde{c}_6 = -\frac{2ie^{\bar{y}_1+2\bar{y}_2}(5(e^{\bar{y}_1} + e^{\bar{y}_2}) + 4(x + 4\xi))}{(e^{\bar{y}_1} + e^{\bar{y}_2})^2 m_Q^3 (e^{\bar{y}_1} + e^{\bar{y}_2} + 4\xi)(e^{\bar{y}_1} + e^{\bar{y}_2} + 2x + 6\xi)},\quad (C53)$$

$$\begin{aligned}\tilde{d}_1 = & 4e^{2\bar{y}_2} Z(e^{\bar{y}_1+2\bar{y}_2} Q^2 - 4e^{\bar{y}_1} m_Q^2 Z^2 + e^{\bar{y}_2}(-e^{2\bar{y}_1} Q^2 + 4m_Q^2 Z^2 + e^{\bar{y}_1} Q^2(x - 2Z + \xi))) \\ & \times \left[m_Q(-e^{2\bar{y}_2} Q^2 + 2e^{\bar{y}_2} Q^2 Z + 4m_Q^2 Z^2)(e^{\bar{y}_2} - x - \xi) \right. \\ & \left. \times (e^{2\bar{y}_2}(e^{\bar{y}_1} Q^2 - 4m_Q^2 Z) - 4e^{\bar{y}_1} m_Q^2 Z(e^{\bar{y}_1} - x + Z - \xi) - 2e^{\bar{y}_2}(e^{\bar{y}_1} Q^2 - 4m_Q^2 Z)(e^{\bar{y}_1} - x + Z - \xi)) \right]^{-1},\end{aligned}\quad (C54)$$

$$\tilde{d}_2 = \frac{8e^{2\bar{y}_2} Z(e^{2\bar{y}_2} Q^2 - 4m_Q^2 Z^2 - e^{\bar{y}_2} Q^2(x + 2Z + \xi))}{m_Q(-e^{2\bar{y}_2} Q^2 + 2e^{\bar{y}_2} Q^2 Z + 4m_Q^2 Z^2)(e^{\bar{y}_2} - x - \xi)(-e^{2\bar{y}_2} Q^2 + 2e^{\bar{y}_2} Q^2(x + Z + \xi) + 4m_Q^2 Z(x + Z + \xi))}.\quad (C55)$$

We may see that all the contributions, as a function of x , include poles; for this reason, all the integrals that include convolution of these coefficient functions with GPDs should be understood in the principal value sense, taking into account the above-mentioned $\xi \rightarrow \xi - i0$ prescription

[40] for contour deformation near the poles. Special points of concern are the contributions c_1, c_2 , which stem from the three-gluon diagrams 11–14 in Fig. 3 and contain singularities $\sim(x - \xi)^{-1}$. These singularities apparently overlap with similar singularities in (C16), leading to the

second-order poles. The integral in the vicinity of such singularities is defined via integration by parts [101],

$$\begin{aligned} \int_{-1}^1 dx \frac{H^g(x, \xi)}{(x \mp \xi \pm i0)^2} &= - \int_{-1}^1 dx H^g(x, \xi) \frac{d}{dx} \left(\frac{1}{x \mp \xi \pm i0} \right) \\ &= - \frac{H^g(x, \xi)}{x \mp \xi \pm i0} \Big|_{-1}^1 \\ &\quad + \int_{-1}^1 dx \frac{\partial_x H^g(x, \xi)}{x \mp \xi \pm i0}, \end{aligned} \quad (\text{C56})$$

and exists only if the derivative $\partial_x H^g(x, \xi)$ is a continuous function near the points $x = \pm \xi$. Fortunately, in the process under consideration, such second-order poles cancel, since near the point $x \approx \xi$ we have for residues

$$\text{Resc}_{x=\xi} = -\text{Resc}_{x=-\xi}. \quad (\text{C57})$$

A careful analysis demonstrates that such singularities occur only in the $z_1 = z_2 = 1/2$ approximation. Beyond that limit, the two poles are separated from each other by a distance $\pm(\frac{1}{4z_a} - z_a)e^{\tilde{y}_a}$ or an equivalent expression, which might be found by the replacement $z_a \rightarrow 1 - z_a$.

Finally, we need to mention that in the limit $Q = 0$ it is possible to express the coefficients (C22)–(C55) in a compact form, as a function of skewedness variable ξ and rapidity difference $\Delta y = y_1 - y_2$. Since photoproduction gives the dominant contribution to the cross section and might present special interest for future phenomenological studies, in the following we provide explicit expressions for this case:

$$a_5 = a_7 = b_1 = \tilde{a}_5 = \tilde{a}_7 = \tilde{b}_1 = 0, \quad (\text{C58})$$

$$a_1 = - \frac{2e^{2\Delta y}(\xi + 1)(\xi + x)}{m_Q^3(e^{\Delta y} + 1)^2(2e^{\Delta y}(\xi + 1) + 4\xi + 3)(\xi(e^{\Delta y}(\xi + 1) + 2\xi + 1) - (e^{\Delta y} + 2)(\xi + 1)x)}, \quad (\text{C59})$$

$$a_2 = \frac{1}{m_Q^3(e^{\Delta y} + 1)^2(4\xi^2 + 7\xi + 3)}, \quad (\text{C60})$$

$$a_3 = \frac{2e^{\Delta y}(2e^{\Delta y} + 1)}{m_Q^3(e^{\Delta y} + 1)^2(e^{\Delta y}(4\xi + 3) + 2(\xi + 1))}, \quad (\text{C61})$$

$$a_4 = \frac{2e^{\Delta y}}{m_Q^3(e^{\Delta y} + 1)^2(4\xi + 3)(e^{\Delta y}(4\xi + 3) + 2(\xi + 1))}, \quad (\text{C62})$$

$$a_6 = \frac{2e^{\Delta y}\xi^2}{m_Q^3(e^{\Delta y} + 1)^2(\xi(2\xi + 1) - 2(\xi + 1)x)(\xi(e^{\Delta y}(\xi + 1) + 2\xi + 1) - (e^{\Delta y} + 2)(\xi + 1)x)}, \quad (\text{C63})$$

$$b_2 = \frac{\xi}{m_Q^3(1 + \cosh(\Delta y))(-\xi^2 + \xi x + x)}, \quad (\text{C64})$$

$$b_3 = \frac{2e^{\Delta y}\xi^2}{m_Q^3(e^{\Delta y} + 1)^2(\xi^2 - (\xi + 1)x)(\xi(2\xi + 1) - 2(\xi + 1)x)}, \quad (\text{C65})$$

$$\begin{aligned} c_1 &= \frac{2e^{2\Delta y}}{(e^{\Delta y} + 1)^3 m_Q^3 (e^{\Delta y}(2\xi + 1) + 4\xi + 3)(e^{\Delta y}(4\xi + 3) + 2\xi + 1)(x - \xi)(\xi + 2(\xi^2 + \xi x + x))} \\ &\quad \times \left[\xi^2(-e^{2\Delta y}(2\xi + 1)(4\xi + 3) + 2e^{\Delta y}(2\xi(\xi + 4) + 5) - 2\xi(4\xi + 7) - 7) - 8(e^{\Delta y} - 1)(\xi + 1)^2 x^2 \right. \\ &\quad \left. + 2e^{\Delta y}\xi x((8\xi^2 + 4\xi - 1)\cosh(\Delta y) - 2(\xi + 1)\sinh(\Delta y) + 2\xi(5\xi + 4) + 1) \right], \end{aligned} \quad (\text{C66})$$

$$c_2 = \frac{\operatorname{sech}^2\left(\frac{\Delta y}{2}\right)}{2m_Q^3(4\xi+3)(x-\xi)(2(\xi+1)x-\xi(2\xi+1))\left((\xi+1)\tanh\left(\frac{\Delta y}{2}\right)-3\xi-2\right)\left((\xi+1)\tanh\left(\frac{\Delta y}{2}\right)+3\xi+2\right)} \times \left[\frac{\xi((4\xi+3)(\sinh(\Delta y)(2\xi(2\xi+1)-(4\xi+3)x)+\cosh(\Delta y)(\xi(2\xi+1)-2(\xi+1)x))+\xi+2(\xi+1)(2\xi^2+\xi x+x))}{\cosh(\Delta y)+1} - 8(\xi+1)^2\sinh^4\left(\frac{\Delta y}{2}\right)\operatorname{csch}^3(\Delta y)(\xi^2-2x^2) \right], \quad (\text{C67})$$

$$c_3 = \frac{2e^{2\Delta y}\xi((2e^{\Delta y}+1)(\xi^2+\xi x+x)-\xi)}{(e^{\Delta y}+1)^3m_Q^3(\xi+2(\xi^2+\xi x+x))(e^{\Delta y}(\xi+2(\xi^2+\xi x+x))+\xi^2+\xi x+x)}, \quad (\text{C68})$$

$$c_4 = \frac{(e^{\Delta y}+1)(\xi+1)\operatorname{sech}^4\left(\frac{\Delta y}{2}\right)}{8m_Q^3(e^{\Delta y}(2\xi+1)+4\xi+3)(e^{\Delta y}(4\xi+3)+2\xi+1)(\xi+2(\xi^2+\xi x+x))((e^{\Delta y}+2)(\xi^2+\xi x+x)+\xi)} \times \left[e^{2\Delta y}(\xi^3(60\xi^3+78\xi^2+32\xi+5)+2(\xi+1)^2x^3+2\xi(\xi+1)(3\xi+4)(10\xi+7)x^2) + e^{2\Delta y}\xi^2(2\xi(3\xi(20\xi+43)+83)+31)x + e^{\Delta y}\xi^2(2\xi(\xi(24\xi+41)+14)-3)x + e^{\Delta y}(\xi^3(\xi(12\xi(2\xi+1)-5)-2)-2(\xi+1)^2x^3+\xi(\xi+1)(4\xi(6\xi+11)+17)x^2) + (2\xi+1)(-\xi^3(2\xi(\xi+4)+3)+2(\xi+1)^2x^3+2\xi(\xi+1)^2x^2-\xi^2(2\xi(\xi+4)+7)x) - e^{3\Delta y}(\xi^2+\xi x+x)(-\xi(14\xi+11)+2\xi x+x)(\xi+2(\xi^2+\xi x+x)) \right] (\xi e^{\Delta y}+(\xi^2+\xi x+x)(1+2e^{\Delta y}))^{-1}, \quad (\text{C69})$$

$$c_5 = \frac{4e^{\Delta y}(\xi(16\xi+21)+4(\xi+1)x)}{(e^{\Delta y}+1)^3m_Q^3(4\xi+5)(\xi(6\xi+7)+2(\xi+1)x)}, \quad (\text{C70})$$

$$d_1 = \frac{4\xi^2\sinh\left(\frac{\Delta y}{2}\right)\left(\cosh\left(\frac{\Delta y}{2}\right)(\xi+2(\xi^2+\xi x+x))-\xi\sinh\left(\frac{\Delta y}{2}\right)\right)^{-1}}{m_Q^3(-3\sinh(\Delta y)(3\xi^2+\xi(x+2)+x)+\cosh(\Delta y)(3\xi^2+\xi(x+4)+x)+3\xi^2+\xi x+x)}, \quad (\text{C71})$$

$$d_2 = -\frac{2e^{\Delta y}\xi^2}{m_Q^3(e^{\Delta y}+1)(-\xi^2+\xi x+x)((e^{\Delta y}+1)(\xi^2+\xi x+x)+\xi)}, \quad (\text{C72})$$

$$\tilde{a}_1 = \frac{2e^{2\Delta y}(\xi+1)(\xi+x)}{m_Q^3(e^{\Delta y}+1)^2(2e^{\Delta y}(\xi+1)+4\xi+3)(\xi(e^{\Delta y}(\xi+1)+2\xi+1)-(e^{\Delta y}+2)(\xi+1)x)}, \quad (\text{C73})$$

$$\tilde{a}_2 = -\frac{1}{m_Q^3(e^{\Delta y}+1)^2(4\xi^2+7\xi+3)}, \quad (\text{C74})$$

$$\tilde{a}_3 = \frac{2e^{\Delta y}(2e^{\Delta y}+1)}{m_Q^3(e^{\Delta y}+1)^2(e^{\Delta y}(4\xi+3)+2(\xi+1))}, \quad (\text{C75})$$

$$\tilde{a}_4 = -\frac{2e^{\Delta y}}{m_Q^3(e^{\Delta y}+1)^2(4\xi+3)(e^{\Delta y}(4\xi+3)+2(\xi+1))}, \quad (\text{C76})$$

$$\tilde{a}_6 = -\frac{\xi^2}{m_Q^3(\cosh(\Delta y)+1)(\xi(2\xi+1)-2(\xi+1)x)(\xi(e^{\Delta y}(\xi+1)+2\xi+1)-(e^{\Delta y}+2)(\xi+1)x)}, \quad (\text{C77})$$

$$\tilde{b}_2 = -\frac{\xi}{m_Q^3(\cosh(\Delta y)+1)(-\xi^2+\xi x+x)}, \quad (\text{C78})$$

$$\tilde{b}_3 = -\frac{\xi^2}{m_Q^3(\cosh(\Delta y) + 1)(-\xi^2 + \xi x + x)(2(\xi + 1)x - \xi(2\xi + 1))}, \quad (C79)$$

$$\tilde{c}_1 = \frac{2e^{2\Delta y}(\xi(e^{2\Delta y}(2\xi + 1)(4\xi + 3) + 2e^{\Delta y}(5\xi(2\xi + 3) + 6) - 4\xi(\xi + 3) - 7) + 8(e^{\Delta y} - 1)(\xi + 1)^2 x)}{m_Q^3(e^{\Delta y} + 1)^3(e^{\Delta y}(2\xi + 1) + 4\xi + 3)(e^{\Delta y}(4\xi + 3) + 2\xi + 1)(\xi + 2(\xi^2 + \xi x + x))}, \quad (C80)$$

$$\begin{aligned} \tilde{c}_2 = & -\frac{2e^{\Delta y}}{m_Q^3(e^{\Delta y} + 1)^3(4\xi + 3)(e^{\Delta y}(2\xi + 1) + 4\xi + 3)(e^{\Delta y}(4\xi + 3) + 2\xi + 1)(\xi(2\xi + 1) - 2(\xi + 1)x)} \\ & \times [e^{3\Delta y}\xi(2\xi + 1)(4\xi + 3) - e^{\Delta y}(-4(2\xi + 1)\xi^2 + \xi + 8(\xi + 1)(3\xi + 2)x) \\ & + e^{2\Delta y}(3\xi(2\xi + 1)^2 - 8(\xi + 1)(3\xi + 2)x) + \xi(2\xi + 1)(4\xi + 3)], \end{aligned} \quad (C81)$$

$$\tilde{c}_3 = -\frac{\operatorname{sech}^4\left(\frac{\Delta y}{2}\right)}{2m_Q^3(4\xi + 3)(\xi(2\xi + 1) - 2(\xi + 1)x)\left((\xi + 1)\tanh\left(\frac{\Delta y}{2}\right) - 3\xi - 2\right)\left((\xi + 1)\tanh\left(\frac{\Delta y}{2}\right) + 3\xi + 2\right)} \quad (C82)$$

$$\times \left(-\xi(\xi + 1)^2 \tanh\left(\frac{\Delta y}{2}\right) + (2\xi + 1)\cosh(\Delta y)(-3\xi^2 + \xi(x - 2) + x) - \xi(3\xi + 2)(4\xi + 3) + (\xi + 1)^2 x\right), \quad (C83)$$

$$\tilde{c}_4 = \frac{2e^{2\Delta y}\xi((2e^{\Delta y} + 1)(\xi^2 + \xi x + x) - \xi)}{m_Q^3(e^{\Delta y} + 1)^3(\xi + 2(\xi^2 + \xi x + x))(e^{\Delta y}(\xi + 2(\xi^2 + \xi x + x)) + \xi^2 + \xi x + x)}, \quad (C84)$$

$$\begin{aligned} \tilde{c}_5 = & -\frac{(e^{\Delta y} + 1)(\xi + 1)\operatorname{sech}^4\left(\frac{\Delta y}{2}\right)(\xi e^{\Delta y} + (\xi^2 + \xi x + x)(1 + 2e^{\Delta y}))^{-1}}{8m_Q^3(e^{\Delta y}(2\xi + 1) + 4\xi + 3)(e^{\Delta y}(4\xi + 3) + 2\xi + 1)(\xi + 2(\xi^2 + \xi x + x))((e^{\Delta y} + 2)(\xi^2 + \xi x + x) + \xi)} \\ & \times \left[e^{2\Delta y}(\xi^3(60\xi^3 + 78\xi^2 + 32\xi + 5) + 2(\xi + 1)^2 x^3 + 2\xi(\xi + 1)(3\xi + 4)(10\xi + 7)x^2) \right. \\ & \left. + e^{\Delta y}(\xi^3(\xi(12\xi(2\xi + 1) - 5) - 2) - 2(\xi + 1)^2 x^3 + \xi(\xi + 1)(4\xi(6\xi + 11) + 17)x^2) \right. \end{aligned} \quad (C85)$$

$$\begin{aligned} & \left. + x\xi^2 e^{2\Delta y}(2\xi(3\xi(20\xi + 43) + 83) + 31) + x\xi^2 e^{\Delta y}(2\xi(\xi(24\xi + 41) + 14) - 3) \right. \\ & \left. + (2\xi + 1)(-\xi^3(2\xi(\xi + 4) + 3) + 2(\xi + 1)^2 x^3 + 2\xi(\xi + 1)^2 x^2 - \xi^2(2\xi(\xi + 4) + 7)x) \right. \\ & \left. - e^{3\Delta y}(\xi^2 + \xi x + x)(-\xi(14\xi + 11) + 2\xi x + x)(\xi + 2(\xi^2 + \xi x + x))\right], \end{aligned} \quad (C86)$$

$$\tilde{c}_6 = -\frac{4e^{\Delta y}(\xi(16\xi + 21) + 4(\xi + 1)x)}{m_Q^3(e^{\Delta y} + 1)^3(4\xi + 5)(\xi(6\xi + 7) + 2(\xi + 1)x)}, \quad (C87)$$

$$\tilde{d}_1 = \frac{2(e^{\Delta y} - 1)\xi^2(e^{\Delta y}(\xi + 1)(\xi + x) + \xi^2 + \xi x + x)^{-1}}{m_Q^3(\xi(-3e^{\Delta y}\xi + e^{2\Delta y}(3\xi + 1) - 6\xi - 5) + (e^{\Delta y} - 2)(e^{\Delta y} + 1)(\xi + 1)x)}, \quad (C88)$$

$$\tilde{d}_2 = \frac{2\xi^2}{m_Q^3(e^{\Delta y} + 1)(-\xi^2 + \xi x + x)(e^{\Delta y}(\xi + 1)(\xi + x) + \xi^2 + \xi x + x)}. \quad (C89)$$

[1] M. Diehl, T. Feldmann, R. Jakob, and P. Kroll, *Nucl. Phys.* **B596**, 33 (2001); **B605**, 647(E) (2001).

[2] K. Goeke, M. V. Polyakov, and M. Vanderhaeghen, *Prog. Part. Nucl. Phys.* **47**, 401 (2001).

[3] M. Diehl, *Phys. Rep.* **388**, 41 (2003).

[4] M. Guidal, H. Moutarde, and M. Vanderhaeghen, *Rep. Prog. Phys.* **76**, 066202 (2013).

[5] D. Boer, M. Diehl, R. Milner, R. Venugopalan, W. Vogelsang, D. Kaplan, H. Montgomery, S. Vigdor, A. Accardi, E. C. Aschenauer *et al.*, [arXiv:1108.1713](https://arxiv.org/abs/1108.1713).

- [6] V. Burkert, L. Elouadrhiri, A. Afanasev, J. Arrington, M. Contalbrigo, W. Cosyn, A. Deshpande, D. Glazier, X. Ji, S. Liuti *et al.*, [arXiv:2211.15746](https://arxiv.org/abs/2211.15746).
- [7] K. Kumericki, S. Liuti, and H. Moutarde, *Eur. Phys. J. A* **52**, 157 (2016).
- [8] B. Pire and L. Szymanowski, *Phys. Rev. Lett.* **115**, 092001 (2015).
- [9] B. Pire, L. Szymanowski, and J. Wagner, *Phys. Rev. D* **95**, 094001 (2017).
- [10] B. Pire and L. Szymanowski, *Phys. Rev. D* **96**, 114008 (2017).
- [11] B. Pire, L. Szymanowski, and J. Wagner, *Phys. Rev. D* **104**, 094002 (2021).
- [12] G. Duplančić, S. Nabeebaccus, K. Passek-Kumerički, B. Pire, L. Szymanowski, and S. Wallon, [arXiv:2212.00655](https://arxiv.org/abs/2212.00655).
- [13] G. Duplančić, K. Passek-Passek-Kumerički, B. Pire, L. Szymanowski, and S. Wallon, *J. High Energy Phys.* **11** (2018) 179.
- [14] R. Boussarie, B. Pire, L. Szymanowski, and S. Wallon, *J. High Energy Phys.* **02** (2017) 054.
- [15] W. Cosyn and B. Pire, *Phys. Rev. D* **103**, 114002 (2021).
- [16] A. Pedrak, B. Pire, L. Szymanowski, and J. Wagner, *Phys. Rev. D* **101**, 114027 (2020).
- [17] B. Pire, L. Szymanowski, and S. Wallon, *Phys. Rev. D* **101**, 074005 (2020).
- [18] A. Pedrak, B. Pire, L. Szymanowski, and J. Wagner, *Phys. Rev. D* **96**, 074008 (2017).
- [19] M. El Beiyad, B. Pire, M. Segond, L. Szymanowski, and S. Wallon, *Phys. Lett. B* **688**, 154 (2010).
- [20] D. Y. Ivanov, B. Pire, L. Szymanowski, and O. V. Teryaev, *Phys. Lett. B* **550**, 65 (2002).
- [21] G. Duplančić, S. Nabeebaccus, K. Passek-Kumerički, B. Pire, L. Szymanowski, and S. Wallon, [arXiv:2212.01034](https://arxiv.org/abs/2212.01034).
- [22] M. El Beiyad, B. Pire, M. Segond, L. Szymanowski, and S. Wallon, *Phys. Lett. B* **688**, 154 (2010).
- [23] R. Boussarie, B. Pire, L. Szymanowski, and S. Wallon, *J. High Energy Phys.* **02** (2017) 054; **10** (2018) 029(E).
- [24] J.-W. Qiu and Z. Yu, *J. High Energy Phys.* **08** (2022) 103.
- [25] J.-W. Qiu and Z. Yu, *Phys. Rev. D* **107**, 014007 (2023).
- [26] J. G. Korner and G. Thompson, *Phys. Lett. B* **264**, 185 (1991).
- [27] M. Neubert, *Phys. Rep.* **245**, 259 (1994).
- [28] G. T. Bodwin, E. Braaten, and G. P. Lepage, *Phys. Rev. D* **51**, 1125 (1995); **55**, 5853(E) (1997).
- [29] F. Maltoni, M. L. Mangano, and A. Petrelli, *Nucl. Phys.* **B519**, 361 (1998).
- [30] N. Brambilla, A. Vairo, and E. Mereghetti, *Phys. Rev. D* **79**, 074002 (2009); **83**, 079904(E) (2011).
- [31] Y. Feng, J. P. Lansberg, and J. X. Wang, *Eur. Phys. J. C* **75**, 313 (2015).
- [32] N. Brambilla *et al.*, *Eur. Phys. J. C* **71**, 1534 (2011).
- [33] P. L. Cho and A. K. Leibovich, *Phys. Rev. D* **53**, 6203 (1996).
- [34] P. L. Cho and A. K. Leibovich, *Phys. Rev. D* **53**, 150 (1996).
- [35] S. P. Baranov, *Phys. Rev. D* **66**, 114003 (2002).
- [36] S. P. Baranov and A. Szczurek, *Phys. Rev. D* **77**, 054016 (2008).
- [37] S. P. Baranov, A. V. Lipatov, and N. P. Zotov, *Phys. Rev. D* **85**, 014034 (2012).
- [38] S. P. Baranov and A. V. Lipatov, *Phys. Rev. D* **96**, 034019 (2017).
- [39] S. P. Baranov, A. V. Lipatov, and N. P. Zotov, *Eur. Phys. J. C* **75**, 455 (2015).
- [40] D. Yu. Ivanov, A. Schafer, L. Szymanowski, and G. Krasnikov, *Eur. Phys. J. C* **34**, 297 (2004).
- [41] M. Vanttinen and L. Mankiewicz, *Phys. Lett. B* **440**, 157 (1998).
- [42] J. Koempel, P. Kroll, A. Metz, and J. Zhou, *Phys. Rev. D* **85**, 051502(R) (2012).
- [43] Z. L. Cui, M. C. Hu, and J. P. Ma, *Eur. Phys. J. C* **79**, 812 (2019).
- [44] S. J. Brodsky, G. Kopp, and P. M. Zerwas, *Phys. Rev. Lett.* **58**, 443 (1987).
- [45] G. P. Lepage and S. J. Brodsky, *Phys. Rev. D* **22**, 2157 (1980).
- [46] C. Berger and W. Wagner, *Phys. Rep.* **146**, 1 (1987).
- [47] M. S. Baek, S. Y. Choi, and H. S. Song, *Phys. Rev. D* **50**, 4363 (1994).
- [48] Y. Bai, S. Lu, and J. Osborne, *Phys. Lett. B* **798**, 134930 (2019).
- [49] W. Heupel, G. Eichmann, and C. S. Fischer, *Phys. Lett. B* **718**, 545 (2012).
- [50] R. J. Lloyd and J. P. Vary, *Phys. Rev. D* **70**, 014009 (2004).
- [51] J. Vijande, N. Barnea, and A. Valcarce, *Int. J. Mod. Phys. A* **22**, 561 (2007).
- [52] J. Vijande, A. Valcarce, and J.-M. Richard, *Few-Body Syst.* **54**, 1015 (2013).
- [53] X. Chen, *Phys. Rev. D* **100**, 094009 (2019).
- [54] A. Esposito and A. D. Polosa, *Eur. Phys. J. C* **78**, 782 (2018).
- [55] R. Cardinale (LHCb Collaboration), *Proc. Sci. LHCP2018* (2018) 191.
- [56] R. Aaij *et al.* (LHCb Collaboration), *J. High Energy Phys.* **10** (2018) 086.
- [57] L. Capriotti (LHCb Collaboration), *J. Phys. Conf. Ser.* **1137**, 012004 (2019).
- [58] R. Aaij *et al.* (LHCb Collaboration), *Sci. Bull.* **65**, 1983 (2020).
- [59] V. P. Goncalves, B. D. Moreira, and F. S. Navarra, *Eur. Phys. J. C* **76**, 103 (2016).
- [60] V. P. Goncalves and R. Palota da Silva, *Phys. Rev. D* **101**, 034025 (2020).
- [61] V. P. Goncalves and M. V. T. Machado, *Eur. Phys. J. C* **49**, 675 (2007).
- [62] S. Baranov, A. Cisek, M. Klusek-Gawenda, W. Schafer, and A. Szczurek, *Eur. Phys. J. C* **73**, 2335 (2013).
- [63] H. Yang, Z. Q. Chen, and C. F. Qiao, *Eur. Phys. J. C* **80**, 806 (2020).
- [64] V. P. Goncalves, B. D. Moreira, and F. S. Navarra, *Eur. Phys. J. C* **76**, 388 (2016).
- [65] S. Andradé, M. Siddikov, and I. Schmidt, *Phys. Rev. D* **105**, 076022 (2022).
- [66] A. Accardi *et al.*, *Eur. Phys. J. A* **52**, 268 (2016).
- [67] Press release at the website of the U.S. Department of Energy: <https://www.energy.gov/articles/us-department-energy-selects-brookhaven-national-laboratory-host-major-new-nuclear-physics>.
- [68] Press release at the website of the Brookhaven National Laboratory (BNL): <https://www.bnl.gov/newsroom/news.php?a=116998>.

- [69] R. Abdul Khalek *et al.*, *Nucl. Phys.* **A1026**, 122447 (2022).
- [70] B. LehmannDronke, P. V. Pobylitsa, M. V. Polyakov, A. Schafer, and K. Goeke, *Phys. Lett. B* **475**, 147 (2000).
- [71] B. Lehmann-Dronke, A. Schafer, M. V. Polyakov, and K. Goeke, *Phys. Rev. D* **63**, 114001 (2001).
- [72] B. Clerbaux and M. V. Polyakov, *Nucl. Phys.* **A679**, 185 (2000).
- [73] M. Diehl, T. Gousset, and B. Pire, [arXiv:hep-ph/9909445](https://arxiv.org/abs/hep-ph/9909445).
- [74] J. Breitweg *et al.* (ZEUS Collaboration), *Eur. Phys. J. C* **6**, 603 (1999).
- [75] A. V. Radyushkin, *Phys. Lett. B* **380**, 417 (1996).
- [76] A. V. Radyushkin, *Phys. Rev. D* **56**, 5524 (1997).
- [77] J. C. Collins and A. Freund, *Phys. Rev. D* **59**, 074009 (1999).
- [78] X. D. Ji, *Phys. Rev. D* **55**, 7114 (1997).
- [79] X. D. Ji and J. Osborne, *Phys. Rev. D* **58**, 094018 (1998).
- [80] S. V. Goloskokov and P. Kroll, *Eur. Phys. J. C* **74**, 2725 (2014).
- [81] A. V. Belitsky, D. Mueller, and A. Kirchner, *Nucl. Phys.* **B629**, 323 (2002).
- [82] A. V. Belitsky and A. V. Radyushkin, *Phys. Rep.* **418**, 1 (2005).
- [83] J. P. Ma and Z. G. Si, *Phys. Lett. B* **647**, 419 (2007).
- [84] X. P. Wang and D. Yang, *J. High Energy Phys.* **06** (2014) 121.
- [85] W. Wang, J. Xu, D. Yang, and S. Zhao, *J. High Energy Phys.* **12** (2017) 012.
- [86] E. Braaten and J. Lee, *Phys. Rev. D* **67**, 054007 (2003); **72**, 099901(E) (2005).
- [87] S. V. Goloskokov and P. Kroll, *Eur. Phys. J. C* **50**, 829 (2007).
- [88] S. V. Goloskokov and P. Kroll, *Eur. Phys. J. C* **53**, 367 (2008).
- [89] S. V. Goloskokov and P. Kroll, *Eur. Phys. J. C* **59**, 809 (2009).
- [90] S. V. Goloskokov and P. Kroll, *Eur. Phys. J. C* **65**, 137 (2010).
- [91] S. V. Goloskokov and P. Kroll, *Eur. Phys. J. A* **47**, 112 (2011).
- [92] V. M. Braun and I. B. Filyanov, *Z. Phys. C* **48**, 239 (1990).
- [93] P. Ball, *J. High Energy Phys.* **01** (1999) 010.
- [94] P. Ball and V. M. Braun, *Phys. Rev. D* **54**, 2182 (1996).
- [95] P. Ball, V. M. Braun, Y. Koike, and K. Tanaka, *Nucl. Phys.* **B529**, 323 (1998).
- [96] P. Ball and V. M. Braun, *Nucl. Phys.* **B543**, 201 (1999).
- [97] S. J. Brodsky, H. C. Pauli, and S. S. Pinsky, *Phys. Rep.* **301**, 299 (1998).
- [98] X. D. Ji, *J. Phys. G* **24**, 1181 (1998).
- [99] V. Shtabovenko, R. Mertig, and F. Orellana, *Comput. Phys. Commun.* **207**, 432 (2016).
- [100] R. Mertig, M. Böhm, and A. Denner, *Comput. Phys. Commun.* **64**, 345 (1991).
- [101] S. P. Baranov, *Phys. Rev. D* **81**, 034021 (2010).